was then normalized by the maximal fluorescence intensity before the electrical stimulation.

### Statistical Analysis

Student's *t*-test was used for comparison of the means of unpaired data. For multiple comparisons, ANOVA followed by Fisher's protected least significant difference (PLSD) was performed.

## RESULTS

### Zinc Dynamics in Mossy Fiber Terminals During Tetanic Stimulation

To observe zinc movement in mossy fiber terminals, intracellular zinc is stained with ZnAF-2 DA, the diacetylated form of ZnAF-2. ZnAF-2 DA taken up by cells is hydrolyzed to ZnAF-2, which cannot permeate the cell membrane. The fluorescent signal was high in the dentate hilus and stratum lucidum, in which mossy fibers of dentate granule cells exist (Fig. 1). When ZnAF-2 was added to hippocampal slices, the fluorescent signal was immediately detected in the dentate hilus and stratum lucidum. The fluorescent signal was also detected around their regions.

Hippocampal slice was doubly stained with ZnAF-2 and Fura-2 AM, and tetanic stimuli at 100 Hz for 1 sec were delivered to the dentate granule cell layer (Fig. 2). Extracellular ZnAF-2 signal was increased with intracellular Fura-2 signal in the stratum lucidum during the stimulation. In the case of the stimulation of the dentate granule cell layer after staining with ZnAF-2 DA, intracellular ZnAF-2 signal was also increased in the stratum lucidum during the stimulation.

### Inhibition of Calcium Signaling by Zinc in Mossy Fiber Terminals During Tetanic Stimulation

To examine zinc action against calcium signaling in mossy fiber terminals, ZnAF-2 DA and calcium orange AM were regionally loaded in the stratum lucidum as shown in Figure 3a. The mossy fibers and associational/commissural fibers were stained with calcium orange, whereas only giant boutons of the mossy fibers were stained with ZnAF-2 (Fig. 3b). Thus, double-stained areas are thought to be giant boutons of the mossy fibers. Tetanic stimuli at 100 Hz for 1 sec were delivered to the dentate granule cell layer, and the change of each fluorescent signal was monitored in double-stained mossy fiber terminals. Intracellular calcium orange signal was significantly increased in mossy fiber terminals during the stimulation. The increase in calcium orange signal was markedly enhanced by addition of 1 mM CaEDTA, a membrane-impermeable zinc chelator, but significantly suppressed by addition of 100 μM $ZnCl_2$ (Fig. 3c).

Intracellular ZnAF-2 signal in mossy fiber terminals was also increased during tetanic stimulation and returned to the basal level immediately after the stimulation (Fig. 3c). The increase in ZnAF-2 signal was significantly attenuated by addition of 1 mM CaEDTA.

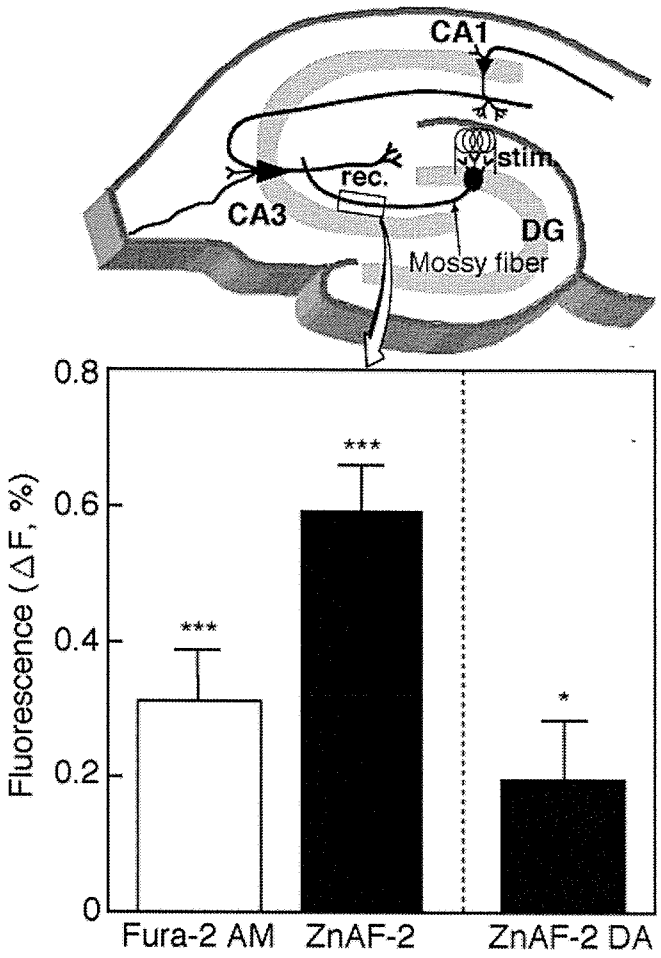


Fig. 2. Zinc movement in the hippocampal synapses during tetanic stimulation. Hippocampal slices were doubly stained with Fura-2 AM and ZnAF-2 (n = 12). Hippocampal slices were also stained with ZnAF-2 DA (n = 21). Tetanic stimuli at 100 Hz for 1 sec were delivered to the dentate granule cell layer, and the fluorescent signals were monitored with a confocal laser scanning microscopic system LSM 510 at the rate of 1 Hz through a ×10 objective, as shown in the illustration. Region of interest (about 10 μm in diameter) was set in the stratum lucidum based on each ZnAF-2 signal. The data represent the increment (%) of fluorescent signal during the stimulation (1 sec) to the basal fluorescent signal just before the stimulation (the mean of 3 sec). Each bar and line represents mean ± SEM. $*P < 0.05$, $***P < 0.001$, vs. basal level before stimulation.

### Inhibition of Vesicular Exocytosis by Zinc in Mossy Fiber Terminals During Tetanic Stimulation

To observe the suppressive zinc action against presynaptic activity, vesicular exocytosis was evaluated by using a fluorescent styryl dye, FM4-64. FM4-64 is taken up into presynaptic vesicles in an activity-dependent manner. Subsequent rounds of exocytosis arising from depolarization lead to the release of the dye from the presynaptic terminals (destaining). Because fluorescence signal originates from vesicular membrane-bound FM4-64, the signal is attenuated by presynaptic activity (Klin-

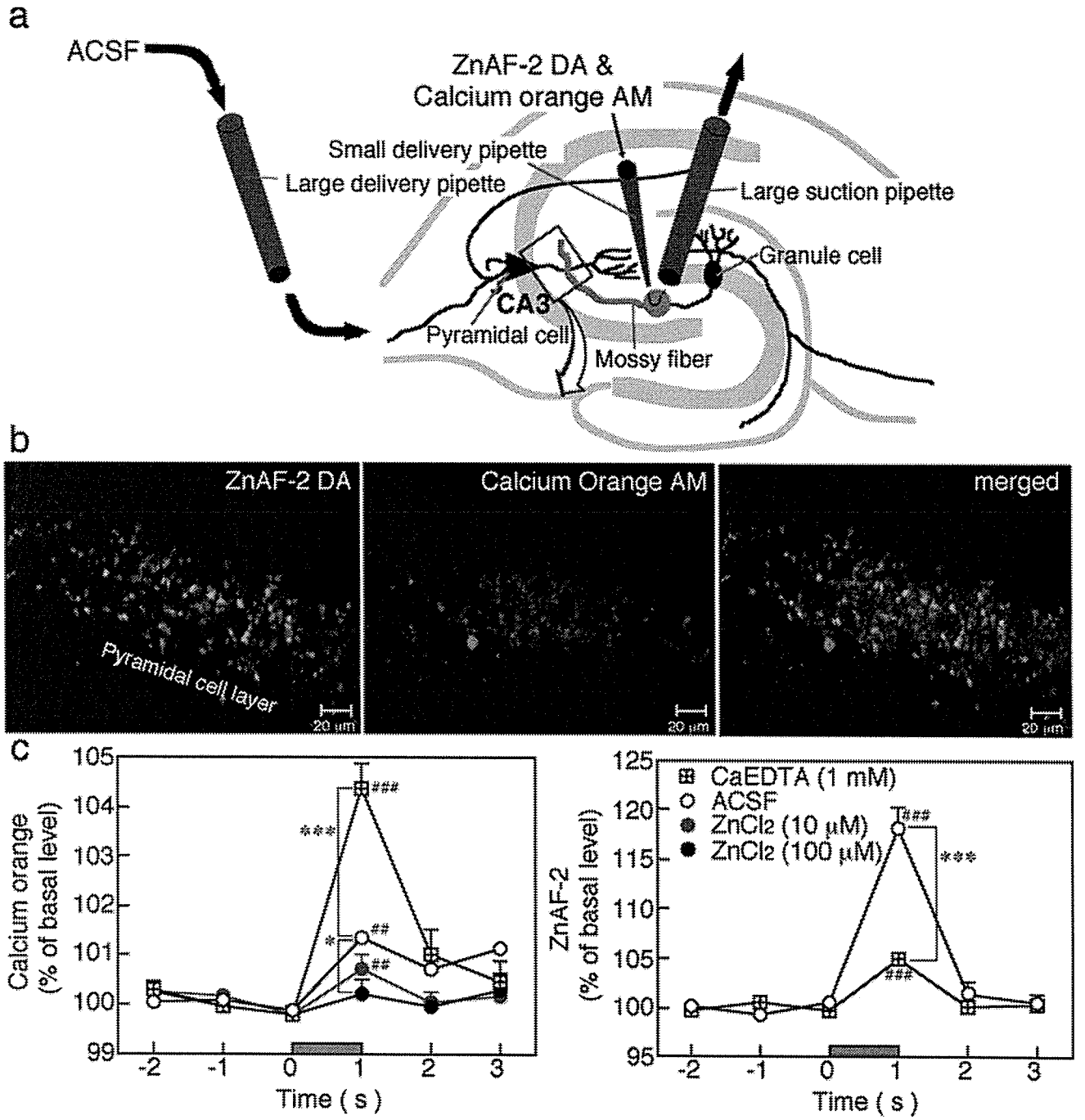


Fig. 3. Inhibition of calcium signaling by zinc in mossy fiber terminals during tetanic stimulation. **a:** Schematic illustration of the procedure. The stratum lucidum was regionally perfused with ZnAF-2 DA and calcium orange AM for mossy fiber terminal labeling. The red square was observed as shown in b. **b:** Giant boutons of mossy fibers were doubly labeled with calcium orange and ZnAF as shown in the merged image. **c:** Tetanic stimuli at 100 Hz for 1 sec were delivered to the dentate granule cell layer in ACSF or reagents in ACSF. The fluorescent signals were monitored with a confocal laser scanning microscopic system LSM 510 at the rate of 1 Hz through a ×20 objective. Region of interest (about 5 μm in diameter) was set in giant boutons of mossy fibers doubly labeled with calcium orange and ZnAF. The data represent the ratio (%) of each fluorescent signal (1 sec) to the basal fluorescent signal (the mean of 3 sec) just before the stimulation. Each point and line represents the mean ± SEM (N = 8–18). The shaded bar indicates the period of the stimulation. $^{*}P < 0.05$, $^{***}P < 0.001$, vs. ACSF group (open circle); $^{\#\#}P < 0.01$, $^{\#\#\#}P < 0.001$, vs. the basal level (the mean of three points just before the stimulation).

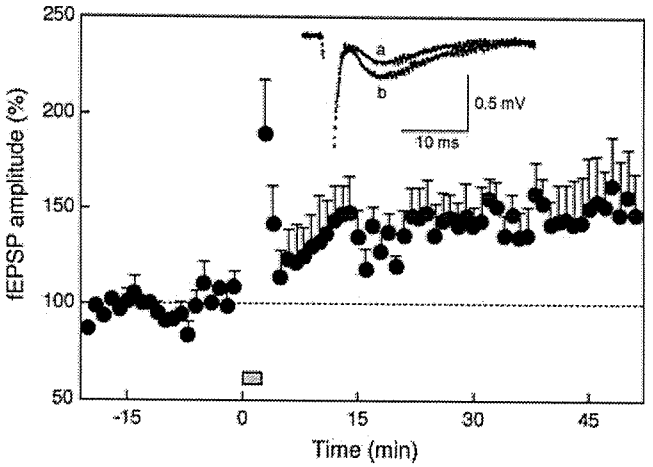


Fig. 4. LTP at mossy fiber-CA3 pyramidal neuron. The mossy fiber-CA3 pyramidal neuron responses were induced by delivery of tetanic stimuli at 10 Hz for 180 sec to the dentate granule cell layer. The shaded bar indicates the period of the stimulation. The superimposed traces are fEPSP recorded before (a) and after (b) tetanic stimulation. The maximal amplitude of the mossy fiber-CA3 fEPSP was calculated and normalized to 30 min basal value (defined as 100%). Each point and line represents the mean ± SEM (N = 6).

gauf et al., 1998; Zakharenko et al., 2001). Tetanic stimuli at 10 Hz for 180 sec, which were used for the exocytosis experiment (Kavalali et al., 1999), were delivered to the dentate granule cells and the mossy fiber-CA3 pyramidal neuron responses were checked by the electrophysiological method. The mean amplitude of fEPSP was 146% ± 16% of the basal level (Fig. 4). To examine zinc's action against vesicular exocytosis in mossy fiber terminals, the activity of mossy fiber terminals doubly stained with ZnAF-2 DA and FM4-64 was evaluated by attenuation of FM4-64 signal during the tetanic stimulation (Fig. 5a). Attenuation of FM4-64 signal in mossy fiber terminals was significantly enhanced by addition of 1 mM CaEDTA but significantly suppressed by addition of 100 μM $ZnCl_2$ (Fig. 5b).

When 50 μM pyrithione, a membrane-permeable zinc chelator, was loaded for 90 sec to the hippocampal slices, approximately 10% of intracellular ZnAF-2 signal was decreased in mossy fiber terminals (data not shown). Therefore, tetanic stimuli at 10 Hz for 180 sec were delivered to the dentate granule cell layer after treatment with pyrithione. The attenuation of FM4-64 signal was significantly enhanced by pretreatment with pyrithione (Fig. 5b).

## DISCUSSION

The extracellular concentration of zinc reached in the stratum lucidum after the release from mossy fiber is a matter of debate. Estimates after tetanic stimulation ranged between 10 and 100 μM (Vogt et al., 2000; Li et al., 2001a), even up to 300 μM under extreme conditions (Assaf and Chung, 1984). To monitor dynamics of synaptic zinc, in the present study the change of ZnAF-2 and ZnAF-2 DA signals was observed by using hippocampal slices. ZnAF-2 has a low $K_D$ value of 2.7 nM for zinc, and its fluorescence is minimally changed in the presence of calcium, magnesium, cadmium, nickel, or other heavy metals (Hirano et al., 2000, 2002). ZnAF-2 also has no apparent toxicity to living cells. These features allow us to study zinc movement associated with neuronal activity in hippocampal slices without interference from calcium, magnesium, and other heavy metals (Ueno et al., 2002). When tetanic stimuli at 100 Hz for 1 sec were delivered to the dentate granule cell layer, both extracellular and intracellular ZnAF-2 signals were increased in the stratum lucidum during the stimulation. It is estimated that the increase in intracellular ZnAF-2 signal is due to the binding of cytosolic ZnAF to zinc retaken up after the release and that the increment in cytosolic signal is more than the decrement in vesicular signal. This idea is supported by the data showing that intracellular ZnAF-2 signal in mossy fiber terminals was significantly decreased during the stimulation in the presence of 1 mM CaEDTA, which chelates zinc in the extracellular fluid. These results suggest that zinc released from mossy fiber terminals during tetanic stimulation is immediately retaken up by the mossy fibers. One millimolar CaEDTA may be effective in chelating zinc released and inhibiting zinc reuptake by mossy fibers. It is likely that the diffusion of zinc released is minimal and that extracellular concentration of zinc after the release is lower than the estimates, except for the synaptic cleft concentration. On the other hand, the translocation of zinc is observed in the CA3 and CA1 of kainate-treated zinc transporter-3-null mice, which lack the histochemically reactive zinc in synaptic vesicles (Lee et al., 2000).

Fig. 5. Inhibition of vesicular exocytosis by zinc in mossy fiber terminals during tetanic stimulation. **a:** Giant boutons of mossy fibers were doubly labeled with FM4-64 and ZnAF as shown in a merged image. **b:** Tetanic stimuli at 10 Hz for 180 sec were delivered to the dentate granule cell layer in ACSF or reagents in ACSF and then single strong stimuli at 100 Hz for 18 sec were delivered to the same position (N = 7–8). Tetanic stimuli (10 Hz, 180 sec) and single strong stimuli (100 Hz, 18 sec) were also delivered to the dentate granule cell layer in ACSF after treatment with 50 μM pyrithione (N = 7–8). Region of interest (about 5 μm in diameter) was set in giant boutons of mossy fibers double-labeled with FM4-64 and ZnAF. The activity-dependent component of FM4-64 signal was measured for each punctum (1 sec) by subtracting its residual fluorescence intensity (<10% of initial intensity) measured after the strong electrical stimulation (100 Hz, 18 sec). FM4-64 signal was then normalized by the maximal fluorescence intensity before tetanic stimulation at 10 Hz. The shaded bar indicates the period of tetanic stimulation at 10 Hz. The activity-dependent component of FM4-64 signal was also measured in the absence of tetanic stimulation as a baseline control (unstimulated group). The data represent the average taken for 3 sec, and each point and line represents the mean ± SEM. $^{**}P < 0.01$, vs. ACSF group 180 sec after the start of tetanic stimulation at 10 Hz.

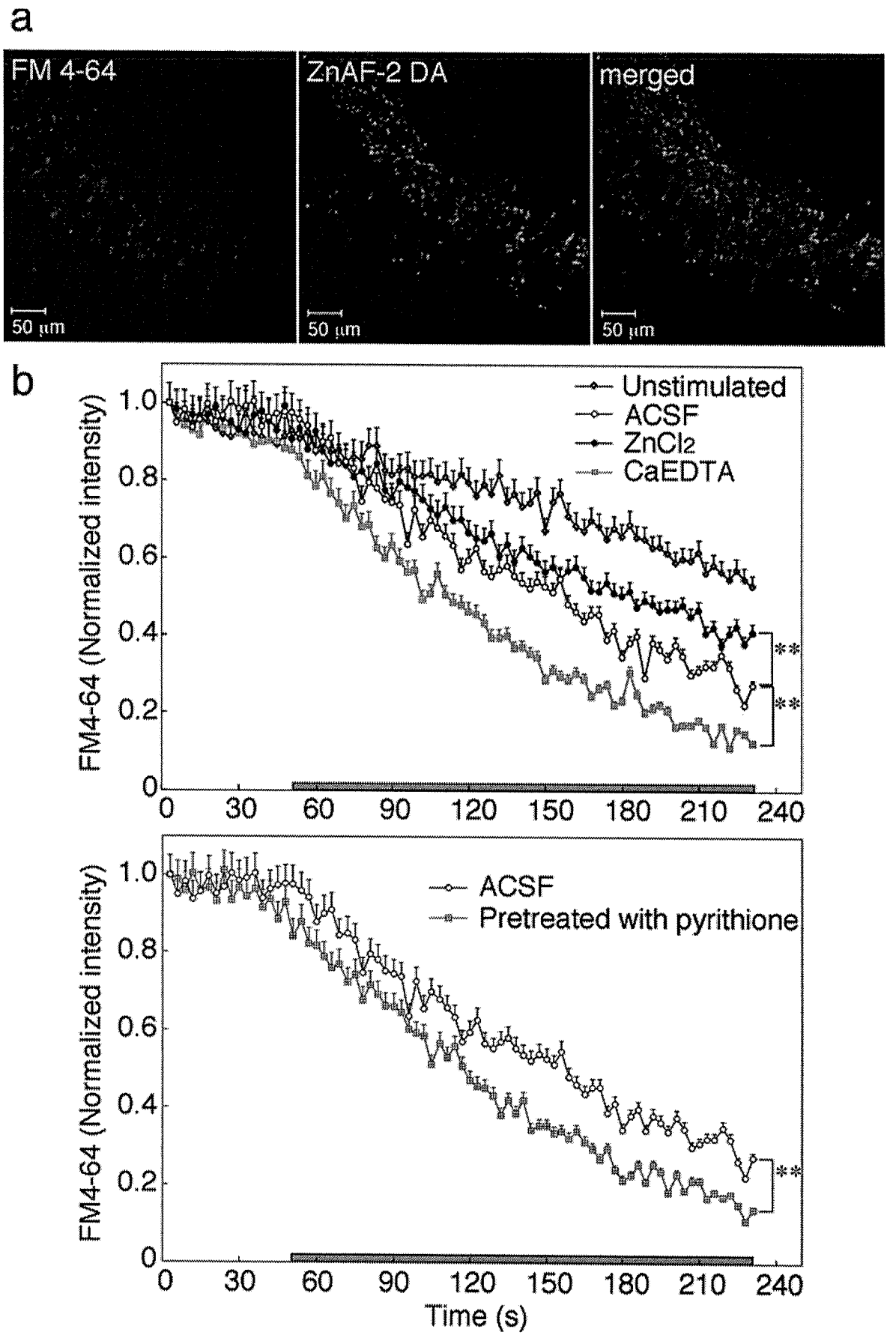
a
FM 4-64
ZnAF-2 DA
merged
50 μm
50 μm
50 μm
b
FM4-64 (Normalized intensity)
Unstimulated
ACSF
ZnCl2
CaEDTA
**
**
0
0.2
0.4
0.6
0.8
1.0
0
30
60
90
120
150
180
210
240
FM4-64 (Normalized intensity)
ACSF
Pretreated with pyrithione
**
Time (s)

Figure 5.

Thus, it is possible that the zinc released originates from sources other than synaptic vesicles.

In the in vivo microdialysis experiment, extracellular glutamate concentrations in the hippocampal CA3 are increased by perfusion with CaEDTA but decreased by perfusion with zinc (Takeda et al., 2003, 2004). Glial glutamate transporter is blocked by zinc (Spiridon et al., 1998). Because this blockade increases extracellular glutamate concentration, it is estimated that zinc efficiently attenuates glutamate release form the neuron terminals. Bancila et al. (2004) showed that exogenously applied zinc inhibits glutamate release via activation of presynaptic ATP-dependent potassium ($K_{ATP}$) channel by using synaptosomal fraction of rat hippocampal CA3. To clarify the presynaptic action of zinc released from mossy fibers, in the present study, endogenous zinc action against presynaptic activity during tetanic stimulation was examined in rat hippocampal slices in the presence of 1 mM CaEDTA.

When mossy fiber terminals were preferentially doubly stained with zinc and calcium indicators, and tetanic stimuli (100 Hz, 1 sec) were delivered to the dentate granule cell layer, the increase in calcium orange signal during the stimulation was enhanced in mossy fiber terminals by addition of CaEDTA and was suppressed by addition of zinc. It is likely that zinc released from mossy fiber terminals suppresses the increase in calcium signal in the presynaptic terminals during tetanic stimulation, followed by suppressive modulation of the presynaptic activity. Mossy fiber zinc may be involved in the mechanism of negative feedback in glutamate release from mossy fibers. Quinta-Ferreira and Matias (2004) demonstrated that N,N,N′,N′-tetrakis(2-pyridylmethyl)ethylenediamine (TPEN; 20 μM), a membrane-permeable zinc chelator, does not prevent the induction of mossy fiber LTP. They also demonstrated that TEPN increases presynaptic calcium signals without affecting the LTP when TPEN was added to the medium after the LTP induction, suggesting that mossy fiber zinc inhibits presynaptic calcium mechanism after the LTP induction. VDCC is involved in calcium influx into presynaptic terminals. Mammalian VDCC currents are blocked by micromolar zinc ($IC_{50}$ = 69 μM; Takahashi and Akaike, 1991; Busselberg et al., 1992). The blockade of VDCC currents and the activation of presynaptic $K_{ATP}$ channel by zinc may be linked with modulation of intracellular calcium signaling pathways. On the other hand, several subtypes of VDCC are present in the mossy fiber boutons (Tokunaga et al., 2004), and zinc is taken up through VDCC and calcium-permeable receptors (Koh and Choi, 1994; Sensi et al., 1997, 1999; Weiss and Sensi, 2000), insofar as intracellular ZnAF-2 signal in the mossy fiber terminals was increased during tetanic stimulation in the present study. It is likely that zinc retaken up, as a signaling factor, also modulates signal transduction pathways via calcium signaling such as protein kinase C and calmodulin in the mossy fiber terminals, followed by the suppression of the increase in calcium signal in the presynaptic terminals during tetanic stimulation. However, the intracellular cross-talk between calcium and zinc signaling is estimated to be complicated (Hedberg et al., 1994). For example, zinc binds to protein kinase C and calmodulin, and zinc release from protein kinase C may be involved in activation of this protein (Baudier et al., 1983; Korichneva et al., 2002). A zinc-sensing receptor triggers the release of intracellular calcium and regulates ion transport (Hershfinkel et al., 2001). Zinc reversibly blocks the influx of capacitative (extracellular) calcium following application of the metabotropic ligands ATP, glutamate, and endothelin-1 (Kresse et al., 2005). Thus, the cross-talk between calcium and zinc signaling in mossy fiber terminals during tetanic stimulation remains to be clarified.

Presynaptic calcium influx through VDCC triggers vesicular exocytosis. It is possible that zinc suppresses vesicular exocytosis. Thus, vesicular exocytosis during tetanic stimulation was examined by using FM4-64, a fluorescent marker of synaptic vesicle recycling. Tetanic stimuli at 10 Hz for 180 sec were delivered to the dentate granule cell layer to evaluate kinetic properties of vesicular exocytosis (Kavalali et al., 1999). Tetanic stimuli at 10 Hz for 180 sec induced mossy fiber LTP. Mossy fiber activity measured with FM4-64 during tetanic stimulation was enhanced by addition of CaEDTA and was suppressed by addition of zinc. Zinc released from mossy fiber terminals during tetanic stimulation may suppress vesicular exocytosis, probably via modulation of the increase in calcium signal in mossy fiber terminals. The effect of CaEDTA during tetanic stimulation might be associated with the increase (about 10%) in fEPSP after LTP induction in the presence of CaEDTA (Vogt et al., 2000; Li et al., 2001b). Mossy fiber activity measured with FM4-64 was also enhanced by pretreatment with pyrithione. Pyrithione is intrinsically nontoxic and has low affinity for zinc ($K_D$, $10^{-6}$; Canzoniero et al., 2003). It is possible that pyrithione blocks intracellular action of zinc, followed by enhancement of vesicular exocytosis in mossy fiber terminals, although further investigation of the effect of pyrithione is necessary. In conclusion, the present study is the first to demonstrate that zinc released from mossy fibers may be a negative-feedback factor against presynaptic activity during tetanic stimulation.

## ACKNOWLEDGMENTS

We thank Noboru Fukasaku and Jun-ichi Kosuge (Synthesis Technology Research Laboratories Daiichi Pure Chemicals Co., Ltd., Kyoto, Japan) for their advice on the use of zinc indicators.

## REFERENCES

Alle H, Jonas P, Geiger JR. 2001. PTP and LTP at a hippocampal mossy fiber–interneuron synapse. Proc Natl Acad Sci U S A 98:14708–14713.

Assaf SY, Chung S-H. 1984. Release of endogeneous $Zn^{2+}$ from brain tissue during activity. Nature 308:734–735.

Bancila V, Nikonenko I, Dunant Y, Bloc A. 2004. Zinc inhibits glutamate release via activation of pre-synaptic $K_{ATP}$ channels and reduces ischaemic damage in rat hippocampus. J Neurochem 90:1243–1250.

Baudier J, Haglid K, Haiech J, Gerard D. 1983. Zinc ion binding to human brain calcium binding proteins, calmodulin and S100b protein. Biochem Biophys Res Commun 114:1138–1146.

Bers DM, Patton C, Nuccitelli R. 1994. A practical guide to the preparation of Ca buffers. Methods Cell Biol 40:3–29.

Breustedt J, Vogt KE, Miller RJ, Nicoll RA, Schmitz D. 2003. Alpha1E-containing $Ca^{2+}$ channels are involved in synaptic plasticity. Proc Natl Acad Sci U S A 100:12450–12455.

Busselberg D, Michael D, Evans ML, Carpenter DO, Haas HL. 1992. Zinc ($Zn^{2+}$) blocks voltage gated calcium channels in cultured rat dorsal root ganglion cells. Brain Res 593:77–81.

Canzoniero LM, Manzerra P, Sheline CT, Choi DW. 2003. Membrane-permeant chelators can attenuate $Zn^{2+}$-induced cortical neuronal death. Neuropharmacology 45:420–428.

Castillo PE, Weisskopf MG, Nicoll RA. 1994. The role of $Ca^{2+}$ channels in hippocampal mossy fiber synaptic transmission and long-term potentiation. Neuron 12:261–269.

Cohen-Kfir E, Lee W, Eskandari S, Nelson N. 2005. Zinc inhibition of γ-aminobutyric acid transporter 4 (GAT4) reveals a link between excitatory and inhibitory neurotransmission. Proc Natl Acad Sci U S A 102:6454–6159.

Cole TB, Martyanova A, Palmiter RD. 2001. Removing zinc from synaptic vesicles dose not impair spatial learning, memory, or sensorimotor functions in the mouse. Brain Res 891:253–265.

Contractor A, Rogers C, Maron C, Henkemeyer M, Swanson GT, Heinemann SF. 2002. Trans-synaptic Eph receptor-ephrin signaling in hippocampal mossy fiber LTP. Science 296:1864–1869.

Danscher G. 1981. Histochemical demonstration of heavy metals. A revised version of the sulphide silver method suitable for both light and electron microscopy. Histochemistry 71:1–16.

Dawson RMC, Elliot DC, Elliot WH, Jones KM. 1986. Data for biochemical research, 3rd ed. New York: Oxford Science.

Frederickson CJ, Klitenick MA, Manton WI, Kirkpatrick JB. 1983. Cytoarchitectonic distribution of zinc in the hippocampus of man and rat. Brain Res 273:335–339.

Hedberg KK, Birrell GB, Mobley PL, Griffith OH. 1994. Transition metal chelator TPEN counteracts phorbol ester-induced actin cytoskeletal disruption in C6 rat glioma cells without inhibiting activation or translocation of protein kinase C. J Cell Physiol 158:337–346.

Hershfinkel M, Moran A, Grossman N, Sekler I. 2001. A zinc-sensing receptor triggers the release of intracellular $Ca^{2+}$ and regulates ion transport. Proc Natl Acad Sci U S A 98:11749–11754.

Hirano T, Kikuchi K, Urano Y, Higuchi T, Nagano T. 2000. Highly zinc-selective fluorescent sensor molecules suitable for biological applications. J Am Chem Soc 122:12399–12400.

Hirano T, Kikuchi K, Urano Y, Nagano T. 2002. Improvement and biological applications of fluorescent probes for zinc, ZnAFs. J Am Chem Soc 124:6555–6562.

Kamiya H, Shinozaki H, Yamamoto C. 1996. Activation of metabotropic glutamate receptor type 2/3 suppresses transmission at rat hippocampal mossy fiber synapses. J Physiol 493:447–455.

Kamiya H, Umeda K, Ozawa S, Manabe T. 2002. Presynaptic $Ca^{2+}$ entry is unchanged during hippocampal mossy fiber long-term potentiation. J Neurosci 22:10524–10528.

Kavalali ET, Klingauf J, Tsien RW. 1999. Activity-dependent regulation of synaptic clustering in a hippocampal culture system. Proc Natl Acad Sci U S A 96:12893–12900.

Klingauf J, Kavalali ET, Tsien RW. 1998. Kinetics and regulation of fast endocytosis at hippocampal synapses. Nature 394:581–585.

Kobayashi K, Manabe T, Takahashi T. 1996. Presynaptic long-term depression at the hippocampal mossy fiber-CA3 synapse. Science 273: 648–650.

Koh JY, Choi DW. 1994. Zinc toxicity on cultured cortical neurons: involvement of N-methyl-D-aspartate receptors. Neuroscience 60:1049–1057.

Korichneva I, Hoyos B, Chua R, Levi E, Hammerling U. 2002. Zinc release from protein kinase C as the common event during activation by lipid second messenger or reactive oxygen. J Biol Cem 277:44327–44331.

Kresse W, Sekler I, Hoffmann A, Peters O, Nolte C, Moran A, Kettenmann H. 2005. Zinc ions are endogenous modulators of neurotransmitter-stimulated capacitative $Ca^{2+}$ entry in both cultured and in situ mouse astrocytes. Eur J Neurosci 21:1626–1634.

Lee JY, Cole TB, Palmiter RD, Koh JY. 2000. Accumulation of zinc in degenerating hippocampal neurons of ZnT3-null mice after seizures: evidence against synaptic vesicle origin. J Neurosci 20:R79.

Li Y, Hough CJ, Suh SW, Sarvey JM, Frederickson CJ. 2001a. Rapid translocation of $Zn^{2+}$ from presynaptic terminals into postsynaptic hippocampal neurons after physiological stimulation. J Neurophysiol 86: 2597–2604.

Li Y, Hough CJ, Frederickson CJ, Sarvey JM. 2001b. Induction of mossy fiber→CA3 long-term potentiation reguires translocation of synaptically released $Zn^{2+}$. J Neurosci 21:8015–8025.

Lu YM, Taverna FA, Tu R, Ackerley CA, Wang YT, Roder J. 2000. Endogenous $Zn^{2+}$ is required for the induction of long-term potentiation at rat hippocampal mossy fiber-CA3 synapses. Synapse 38:187–197.

Mellor J, Nicoll RA. 2001. Hippocampal mossy fiber LTP is independent of postsynaptic calcium. Nat Neurosci 4:125–126.

Nicoll RA, Malenka RC. 1995. Contrasting properties of two forms of long-term potentiation in the hippocampus. Nature 377:115–118.

Paoletti P, Ascher P, Neyton J. 1997. High-affinity zinc inhibition of NMDA NR1-NR2A receptors. J Neurosci 17:5711–5725.

Peters S, Koh J, Choi DW. 1987. Zinc selectively blocks the action of N-methyl-d-aspartate on cortical neurons. Science 236:589–593.

Quinta-Ferreira ME, Matias CM. 2004. Hippocampal mossy fiber calcium transients are maintained during long-term potentiation and are inhibited by endogenous zinc. Brain Res 1004:52–60.

Rassendren FA, Lory P, Pin JP, Nargeot J. 1990. Zinc has opposite effects on NMDA and non-NMDA receptors expressed in Xenopus oocytes. Neuron 4:733–740.

Regehr WG, Tank DW. 1991. Selective fura-2 loading of presynaptic terminals and nerve cell processes by local perfusion in mammalian brain slice. J Neurosci Methods 37:111–119.

Sensi SL, Canzoniero LM, Yu SP, Ying HS, Koh JY, Kerchner GA, Choi DW. 1997. Measurement of intracellular free zinc in living cortical neurons: routes of entry. J Neurosci 17:9554–9564.

Sensi SL, Yin HZ, Carriedo SG, Rao SS, Weiss JH. 1999. Preferential $Zn^{2+}$ influx through $Ca^{2+}$-permeable AMPA/kainate channels triggers prolonged mitochondrial superoxide production. Proc Natl Acad Sci U S A 96:2414–2419.

Sindreu CB, Varoqui H, Erickson JD.Perez-Clausell J. 2003. Boutons containing vesicular zinc define a subpopulation of synapses with low AMPAR content in rat hippocampus. Cereb Cortex 13:823–829.

Smart TG, Xie X, Krishek BJ. 1994. Modulation of inhibitory and excitatory amino acid receptor ion channels by zinc. Prog Neurobiol 42:393–341.

Spiridon M, Kamm D, Billups B, Mobbs P, Attwell D. 1998. Modulation by zinc of the glutamate transporters in glial cells and cones isolated from the tiger salamander retina. J Physiol 506:363–376.

Takahashi K, Akaike N. 1991. Calcium antagonist effects on low-threshold (T-type) calcium current in rat isolated hippocampal CA1 pyramidal neurons. J Pharmacol Exp Ther 256:169–175.

Takeda A, Minami A, Seki Y, Oku N. 2003. Inhibitory function of zinc against excitation of hippocampal glutamatergic neurons. Epilepsy Res 57:169–174.

Takeda A, Minami A, Seki Y, Oku N. 2004. Differential effects of zinc on glutamatergic and GABAergic neurotransmitter systems in the hippocampus. J Neurosci Res 75:225–229.

Tokunaga T, Miyazaki K, Koseki M, Mobarakeh JI, Ishizuka T, Yawo H. 2004. Pharmacological dissection of calcium channel subtype-related components of strontium inflow in large mossy fiber boutons of mouse hippocampus. Hippocampus 14:570–585.

Traynelis SF, Burgess MF, Zheng F, Lyuboslavsky P, Powers JL. 1998. Control of voltage-independent zinc inhibition of NMDA receptors by the NR1 subunit. J Neurosci 18:6163–6175.

Ueno S, Tsukamoto M, Hirano T, Kikuchi K, Yamada MK, Nishiyama N, Nagano T, Matsuki N, Ikegaya Y. 2002. Mossy fiber $Zn^{2+}$ spillover modulates heterosynaptic N-methyl-D-aspartate receptor activity in hippocampal CA3 circuits. J Cell Biol 158:215–220.

Vandenberg RJ, Mitrovic AD, Johnston GA. 1998. Molecular basis for differential inhibition of glutamate transporter subtypes by zinc ions. Mol Pharmacol 54:189–196.

Vogt K, Mellor J, Tong G, Nicoll R. 2000. The actions of synaptically released zinc at hippocampal mossy fiber synapses. Neuron 26: 187–196.

Wang H, Storm DR. 2003. Calmodulin-regulated adenylyl cyclases: cross-talk and plasticity in the central nervous system. Mol Pharmacol 63:463–468.

Wang J, Yeckel MF, Johnston D, Zucker RS. 2004. Photolysis of postsynaptic caged $Ca^{2+}$ can potentiate and depress mossy fiber synaptic responses in rat hippocampal CA3 pyramidal neurons. J Neurophysiol 91:1596–1607.

Weiss JH, Sensi SL. 2000. $Ca^{2+}$-$Zn^{2+}$ permeable AMPA or kainate receptors: possible key factors in selective neurodegeneration. Trends Neurosci 23:365–371.

Westbrook GL, Mayer ML. 1987. Micromolar concentrations of $Zn^{2+}$ antagonize NMDA and GABA responses of hippocampal neurons. Nature 328:640–643.

Williams S, Johnston D. 1989. Long-term potentiation of hippocampal mossy fiber synapses is blocked by postsynaptic injection of calcium chelators. Neuron 3:583–588.

Xie X, Smart TG. 1994. Modulation of long-term potentiation in rat hippocampal pyramidal neurons by zinc. Pflugers Arch 427:481–486.

Yeckel MF, Kapur A, Johnston D. 2001. Multiple forms of LTP in hippocampal CA3 neurons use a common postsynaptic mechanism. Nat Neurosci 2:625–633.

Zakharenko SS, Zablow L, Siegelbaum SA. 2001. Visualization of changes in presynaptic function during long-term synaptic plasticity. Nat Neurosci 4:711–717.

The EMBO Journal (2006) 25, 4596–4604 | © 2006 European Molecular Biology Organization | All Rights Reserved 0261-4189/06
www.embojournal.org

THE EMBO JOURNAL

# The regulator of the $F_1$ motor: inhibition of rotation of cyanobacterial $F_1$-ATPase by the ε subunit

**Hiroki Konno[1,2], Tomoe Murakami-Fuse[1,2], Fumihiko Fujii[3], Fumie Koyama[1,2], Hanayo Ueoka-Nakanishi[2,4], Chan-Gi Pack[3], Masataka Kinjo[3] and Toru Hisabori[1,2,*]**

[1]Chemical Resources Laboratory, Tokyo Institute of Technology, Nagatsuta, Midori-ku, Yokohama, Japan, [2]ATP System Project, Exploratory Research for Advanced Technology (ERATO), Japan Science and Technology Corporation (JST), Nagatsuta-cho, Midori-ku, Yokohama, Japan and [3]Laboratory of Supramolecular Biophysics, Research Institute for Electronic Science, Hokkaido University, Kita-ku, Sapporo, Hokkaido, Japan

**The chloroplast-type $F_1$ ATPase is the key enzyme of energy conversion in chloroplasts, and is regulated by the endogenous inhibitor ε, tightly bound ADP, the membrane potential and the redox state of the γ subunit. In order to understand the molecular mechanism of ε inhibition, we constructed an expression system for the $\alpha_3\beta_3\gamma$ subcomplex in thermophilic cyanobacteria allowing thorough investigation of ε inhibition. ε Inhibition was found to be ATP-independent, and different to that observed for bacterial $F_1$-ATPase. The role of the additional region on the γ subunit of chloroplast-type $F_1$-ATPase in ε inhibition was also determined. By single molecule rotation analysis, we succeeded in assigning the pausing angular position of γ in ε inhibition, which was found to be identical to that observed for ATP hydrolysis, product release and ADP inhibition, but distinctly different from the waiting position for ATP binding. These results suggest that the ε subunit of chloroplast-type ATP synthase plays an important regulator for the rotary motor enzyme, thus preventing wasteful ATP hydrolysis.**

*The EMBO Journal* (2006) **25**, 4596–4604. doi:10.1038/sj.emboj.7601348; Published online 14 September 2006
*Subject Categories*: cellular metabolism
*Keywords*: ATP synthase; ADP inhibition; $CF_1$; rotation; ε inhibition

## Introduction

$F_0F_1$ ATP synthase synthesizes ATP from ADP and inorganic phosphate by way of the proton motive force (*pmf*) generated across the cytoplasmic membranes of bacteria, thylakoid membranes of chloroplasts and inner membranes of mitochondria (Senior, 1990; Boyer, 1997; Yoshida *et al*, 2001). This enzyme can transport protons to generate *pmf* when it hydrolyzes ATP. The enzyme consists of the membrane-embedded portion $F_0$ and the water-soluble portion $F_1$. $F_0$ is composed of three different subunits, *a*, *b* and *c* with a stoichiometry of $a_1b_2c_{10-14}$ (Senior, 1990; Stock *et al*, 1999; Seelert *et al*, 2000; Jiang *et al*, 2001; Mitome *et al*, 2004; Meier *et al*, 2005), and constitutes the proton translocation device. $F_1$ is composed of five different subunits designated α to ε with a stoichiometry of $\alpha_3\beta_3\gamma_1\delta_1\varepsilon_1$ (Yoshida *et al*, 1979). The minimum catalytic core, which maintains the property of $F_1$-ATPase, is $\alpha_3\beta_3\gamma$ (Kaibara *et al*, 1996; Hisabori *et al*, 1997; Matsui *et al*, 1997; Du *et al*, 2001), and the catalytic sites reside on each of the three β subunits at the interface with the α subunits (Abrahams *et al*, 1994). The rotary catalysis mechanism was first proposed by PD Boyer and co-workers based on detailed analysis of the kinetics of $F_1$-ATPase activity (Grubmeyer *et al*, 1982). Following determination of the central axis structure of the γ subunit in the $\alpha_3\beta_3$ hexagon (Abrahams *et al*, 1994), the rotation of the γ subunit during ATP hydrolysis was examined by biochemical cross-linking (Duncan *et al*, 1995) and polarized fluorescence experiments (Sabbert *et al*, 1996). Finally, by single molecule observation, the rotation of the γ subunit was conclusively determined to be coupled with ATP hydrolysis (Noji *et al*, 1997, 1999; Hisabori *et al*, 1999; Omote *et al*, 1999). Thorough analysis of rotation of the γ subunit revealed that the γ subunit rotates with discrete 120° step per single molecule ATP consumption and this 120° step consists of further 80° and 40° substeps (Yasuda *et al*, 1998, 2001). This 80° substep was recently revealed to be induced by ATP binding, whereas ATP cleavage and product release result in a subsequent additional 40° substep (Yasuda *et al*, 2001; Shimabukuro *et al*, 2003).

As ATP synthesis is a key reaction required to maintain a number of metabolic pathways, the $F_0F_1$ complex must be subject to various regulatory mechanisms required to modulate its activity, in order to optimally accommodate changes in environmental conditions. ADP inhibition of the ATP hydrolysis activity is a common regulatory mechanism that has been found to occur in most species; in such a mechanism, the ATP hydrolysis reaction is inhibited by tight binding of ADP-Mg to the catalytic site(s) (Minkov *et al*, 1979; Bar-Zvi and Shavit, 1982; Vasilyeva *et al*, 1982; Malyan and Vitseva, 1983; Feldman and Boyer, 1985; Zhou *et al*, 1988; Digel *et al*, 1996; Matsui *et al*, 1997). Recently, this type of inhibition has been assigned to the pause of the rotation motion at 80° within the 120° catalytic step (Hirono-Hara *et al*, 2001, 2005). Another regulatory mechanism for the ATP hydrolysis reaction is brought about by the intrinsic inhibitory function of the ε subunit (ε inhibition), which is well characterized in bacteria and in chloroplasts (Nelson *et al*, 1972; Richter *et al*, 1984; Aggeler and Capaldi, 1996; Kato *et al*, 1997; Nowak

*Corresponding author. Chemical Resources Laboratory, Tokyo Institute of Technology, Nagatsuta 4259-R1-8, Midori-Ku, Yokohama, Kanagawa 226-8503, Japan. Tel.: +81 45 924 5234; Fax: +81 45 924 5277; E-mail: thisabor@res.titech.ac.jp
[4]Present address: Laboratory of Cell Dynamics, Graduate School of Bioagricultural Sciences, Nagoya University, Nagoya 464-8601, Japan

**Received: 29 June 2006; accepted: 22 August 2006; published online: 14 September 2006**

*et al*, 2002). Both ADP inhibition and ε inhibition may not affect the ATP synthesis activity of $F_oF_1$ (Bald *et al*, 1998; Tsunoda *et al*, 2001). However, the ε subunit of $F_1$ from thermophilic *Bacillus* PS3 ($TF_1$) is known to rotate with the γ subunit and the rotation speed of the ε subunit attached to the γ subunit is not significantly different to that of the γ subunit without ε (Kato-Yamada *et al*, 1998), and inhibition of rotation of the γ subunit caused by ε inhibition has not been characterized in depth at the single molecule level. Furthermore, rotation of the ε subunit in *Escherichia coli* $F_oF_1$ has been observed by FRET measurement (Zimmermann *et al*, 2005). Recently, Nakanishi-Matsui *et al* (2005) reported the inhibition of rotation of the γ subunit by the ε subunit in *E. coli* $F_1$-ATPase ($EF_1$). They observed a distinct increase in the pausing period of the γ subunit during rotation caused by addition of the ε subunit. However, thorough analysis of inhibition by the bacterial ε subunit appears difficult because inhibition shows a complicated kinetic profile based on the conformational change of the ε subunit by ATP during inhibition of the catalytic reaction (Aggeler and Capaldi, 1996; Kato-Yamada *et al*, 2000; Suzuki *et al*, 2003; Iino *et al*, 2005).

In contrast, ε inhibition of the chloroplast-type $F_1$-ATPase is independent of ATP concentration, and ATP hydrolysis activity is inhibited by addition of ε subunit alone to the ε-free complex (Richter *et al*, 1984). However, the effect of ε binding on the $CF_1$ complex has not been studied from the point of view of rotation because of the lack of an enzyme complex that can be suitably manipulated. For the study of $CF_1$ complex at the molecular level, cyanobacterial $F_1$-ATPase is a suitable alternative, as the active enzyme complex can be reconstituted from the recombinant individual subunits α, β, γ, δ and ε (Steinemann *et al*, 1995). In addition, insertion of a 'chloroplast-like' regulatory segment responsible for thiol modulation into the γ subunit of $F_oF_1$-ATPase of the cyanobacterium *Synechocystis* sp. PCC6803 at the chromosome level can be used to generate a redox-sensitive $F_oF_1$, which is one of the main distinguishing features of the chloroplast-type ATP synthase *in vivo* (Werner-Grune *et al*, 1994; Krenn *et al*, 1995).

In order to carry out a detailed study on the effect of the ε subunit on γ subunit rotation, we prepared a 'purpose-built' $F_1$-ATPase $\alpha_3\beta_3\gamma$ complex using an *E. coli*-based expression system for synthesis of the thermophilic cyanobacterial ATP synthase complex, which possesses similar properties to the chloroplast ATPase.

## Results

### *Inhibition of ATPase activity of thermophilic cyanobacterial $\alpha_3\beta_3\gamma$ complex by the ε subunit*

The $\alpha_3\beta_3\gamma$ complex of *Thermosynecoccus elongatus* was overexpressed in *E. coli* BL21(DE3)*uncΔ702* strains and purified as described (see Materials and methods). Using this complex, we first determined whether the cyanobacterial $F_1$ subcomplex has similar properties to the chloroplast-type $F_1$-ATPase in terms of ε inhibition. In the previous study, we found that the ATPase activity of the chimeric complex comprised of the thermophilic bacterial α and β subunits and the spinach chloroplast γ subunit became insensitive to ε subunit inhibition upon deletion of the specific additional region of the chloroplast-type γ subunit that contains the two

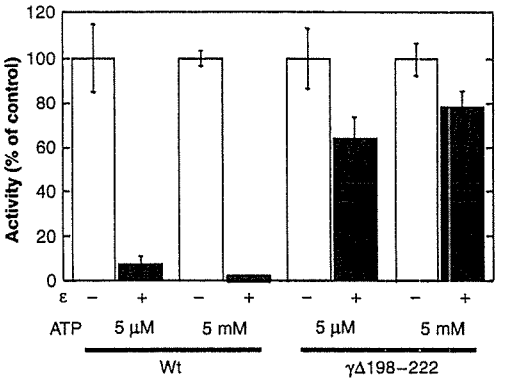


**Figure 1** Effect of the ε subunit on the ATP hydrolysis activities of $\alpha_3\beta_3\gamma_{wild}$ and $\alpha_3\beta_3\gamma_{\Delta198-222}$. $\alpha_3\beta_3\gamma$ subcomplexes (400 nM) were incubated with (closed bar) or without (open bar) 1 μM ε subunit for 6 min at 40°C, and the ATP hydrolysis activity was measured in the presence of ATP regenerating system at 40°C. For the assay, 27 nM wild-type complex and 9 nM $\alpha_3\beta_3\gamma_{\Delta198-222}$ were used.

regulatory cysteines (Hisabori *et al*, 1998). As this result demonstrated the significance of the contribution of additional region of the γ subunit on ε inhibition, we hereby prepared a similar mutant of the cyanobacterial $\alpha_3\beta_3\gamma$ complex, $\alpha_3\beta_3\gamma_{\Delta198-222}$ (Figure 1B in the Supplementary data). The ATPase activity of $\alpha_3\beta_3\gamma_{\Delta198-222}$ was inhibited by 20% by the ε subunit when the enzyme activity was measured in the presence of 5 mM ATP, whereas the extent of inhibition was slightly higher when 5 μM ATP was used (Figure 1). In contrast, the wild-type $\alpha_3\beta_3\gamma$ complex was completely inhibited by the ε subunit irrespective of the ATP concentrations. This strong inhibitory effect under high ATP concentration was very different from that observed for the thermophilic bacterial enzyme (Kato-Yamada *et al*, 1999), but similar to that observed for the chloroplast-type ATPase (Richter *et al*, 1984).

In order to determine the cause of the reduction in the extent of the ε inhibition in the $\alpha_3\beta_3\gamma_{\Delta198-222}$ complex, we calculated the apparent $K_D$ values of the interaction between ε and the $\alpha_3\beta_3\gamma$ complex based on the extent of inhibition of ATP hydrolysis activity of the complex in the presence of various concentrations of the ε subunit (Figure 2A). The estimated $K_D$ values were $2.1\pm0.3$ nM for the wild type and $4.2\pm0.9$ nM for the mutant complex. To confirm the difference in affinity, we then examined the binding of the ε subunit to this $\alpha_3\beta_3\gamma_{\Delta198-222}$ complex using fluorescence correlation spectroscopy (FCS), a valuable method that allows the measurement of the affinity between two protein molecules in solution. For this FCS measurement, a Cys residue was introduced into the ε subunit at the position of Q100 ($\varepsilon_{Q100C}$) and was labeled with Alexa Fluor 488-$C_5$-maleimide. This mutation and the fluorescent dye used did not affect ε inhibition (see the Supplementary Figure 2). This direct binding measurement showed that the affinity between the ε subunit and the complex decreased 3.5-fold by deletion of the additional region of the γ subunit (Figure 2B). The $K_D$ values obtained were $12.5\pm3.2$ nM for the wild type and $44\pm7.2$ nM for the mutant complex. As ε inhibition of the $\alpha_3\beta_3\gamma_{\Delta198-222}$ complex did not increase even in the presence of 1 μM ε subunit (a much higher concentration than the observed $K_D$ value), we concluded that the deleted portion of the γ subunit must play a significant role in ε-induced

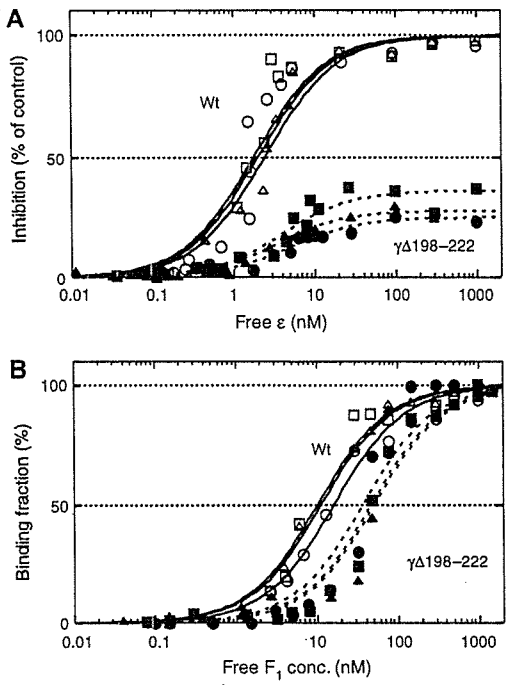


**Figure 2** Binding of the ε subunit to the $\alpha_3\beta_3\gamma_{wild}$ and $\alpha_3\beta_3\gamma_{\Delta198-222}$ complexes. (**A**) The extent of inhibition of the ATPase activity of the $\alpha_3\beta_3\gamma_{wild}$ ('Wt', open symbol) and $\alpha_3\beta_3\gamma_{\Delta198-222}$ ('$\gamma_{\Delta198-222}$', closed symbol) complexes were measured in the presence of various concentrations of the ε subunit. The results from three independent experiments (circle, triangle and square) are plotted against the concentration of free ε subunit (see 'Materials and methods'). Lines were calculated based on the $K_D$ values obtained from the independent measurements above for $\alpha_3\beta_3\gamma_{wild}$ ('Wt', solid line) and for $\alpha_3\beta_3\gamma_{\Delta198-222}$ ('$\gamma_{\Delta198-222}$', dotted line). (**B**) Binding of the ε subunit to the $\alpha_3\beta_3\gamma$ complex was measured by FCS method as a function of the concentration of $\alpha_3\beta_3\gamma_{wild}$ ('Wt', open symbol) and $\alpha_3\beta_3\gamma_{\Delta198-222}$ ('$\gamma_{\Delta198-222}$', closed symbol). For the measurements, the fluorescence-labeled ε was fixed at 5 nM. The complex and the ε subunit were incubated for 60 min at 40°C, and the FCS measurement was carried out at 37°C. The results from three independent experiments (circle, triangle and square) are plotted. The titration curves for $\alpha_3\beta_3\gamma_{wild}$ ('Wt', solid line) and for $\alpha_3\beta_3\gamma_{\Delta198-222}$ ('$\gamma_{\Delta198-222}$', dotted line) were fitted as described (see Materials and methods).

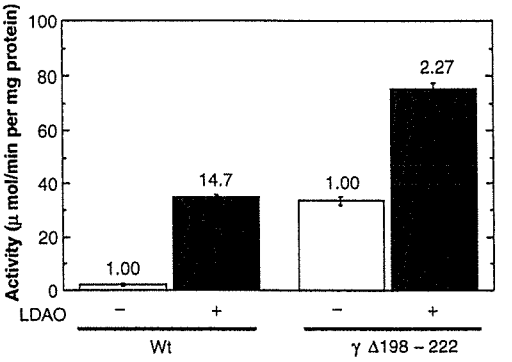


**Figure 3** Effect of LADO on the ATP hydrolysis activity of the $\alpha_3\beta_3\gamma_{wild}$ and $\alpha_3\beta_3\gamma_{\Delta198-222}$ complexes. ATP hydrolysis of $\alpha_3\beta_3\gamma_{wild}$ and $\alpha_3\beta_3\gamma_{\Delta198-222}$ was measured as described in Figure 1 in the presence (closed bar) and the absence (open bar) of 0.1% (w/v) LADO. Steady-state activity was determined from the slope from 180 to 200 s after addition of the enzyme solutions, and the results of three independent experiments were averaged. The extent of the activation by the addition of LADO is indicated on the bars.

inhibition, although the reduced inhibitory effect of the ε subunit on the mutant complex might be in part due to decreased binding of the ε subunit. To further dissect the properties of the mutant γ subunit, we measured the enzyme activity of the wild type and $\alpha_3\beta_3\gamma_{\Delta198-222}$ complex in the presence and absence of the nonionic detergent lauryldimethylamine oxide (LADO) (Figure 3). LADO is a useful indicator of the susceptibility of an enzyme to ADP inhibition (Paik *et al*, 1993). The mutant was found to be less activated in the presence of LADO, suggesting that, in comparison to the wild type, the $\alpha_3\beta_3\gamma_{\Delta198-222}$ complex may be less prone to ADP inhibition. These results suggest that the additional region of the chloroplast-type γ subunit is an important determinant of the susceptibility of the complex to both ε inhibition and ADP inhibition.

### *Enzyme preparation for single molecule observation and its inhibition by the ε subunit*

To observe ε inhibition of rotation of the γ subunit in detail, two cysteine residues were introduced at the surface of the γ subunit. These two cysteines were used as an attachment site for the beads that are used as a probe to observe the movement of γ. After screening the γ subunit for mutations that would not affect ε-induced inhibition, amino-acid positions corresponding to Gly-112 and Ala-125 were used as recipients for introduction of the required cysteine residues, in addition to the substitution of Lys-221 to Ser, which is located in the additional region. Lys-221 appears to be a critical residue of this region of the enzyme, because substitution of this residue to Ser resulted in an increase in ATPase activity, and reduced the susceptibility of the enzyme to ADP inhibition state as observed for the $\alpha_3\beta_3\gamma_{\Delta198-222}$ complex. However, the remarkable difference between the K221S mutation and $\gamma_{\Delta198-222}$ was that the former showed no significant difference in the extent of ε inhibition (see Figure 1 in contrast to Table I of the Supplementary data). The complex containing the three γ subunit mutations G112C, A125C and K221S (designated $\alpha_3\beta_3\gamma$-rot) showed 10-fold higher activity than the wild-type complex (Table I of the Supplementary data), and was used for the rotation experiments. Specific biotinylation of the introduced cysteines was confirmed by Western blotting using a streptavidin-conjugated alkaline phosphatase (Figure 3 in the Supplementary data).

Having prepared the experimental system described above, we sought to investigate the kinetic properties of $\alpha_3\beta_3\gamma$-rot ATPase activity and its inhibition by the ε subunit (Figure 4A). The $K_M$ and $V_{max}$ values obtained for $\alpha_3\beta_3\gamma$-rot were the following: 85.8 μM and 44.3 $s^{-1}$ in the absence of the ε subunit, 52.2 μM and 32.1 $s^{-1}$ in the presence of 3 nM ε subunit, and 66.5 μM and 21.4 $s^{-1}$ in the presence of 5 nM ε subunit. The ε subunit was thus found to inhibit the ATPase activity noncompetitively. Figure 4B shows a typical time course for the ε-induced inhibition. The decrease in the activity following addition of ε occurred within a few minutes and the obtained curve fitted to a single exponential function. The gradual decrease in activity indicates binding of the ε subunit to the complex, and the binding rate constant, $k_{obs}$, was calculated from these curves. Based on the observed linear relation of $k_{obs}$ against the ε concentrations, a $k_{on}$ value of $4.9 \times 10^5\ M^{-1}\ s^{-1}$ was obtained (Figure 4C). Although the extrapolated intercept of Figure 4C gives the theoretical $k_{off}$

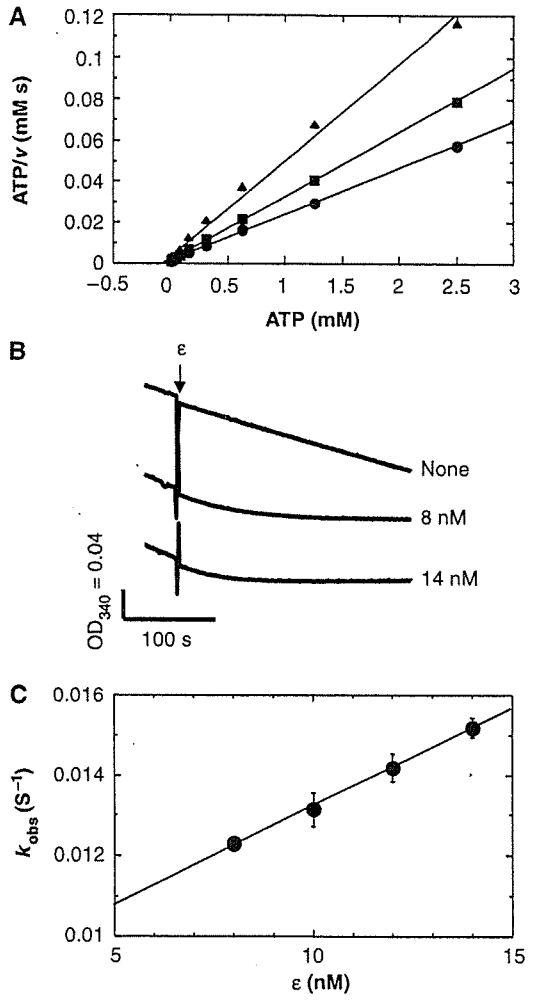


**Figure 4** Inhibition of ATP hydrolysis activity of the $\alpha_3\beta_3\gamma$-rot complex by the ε subunit. (**A**) S/v-S plots of the rates of ATP hydrolysis with 5–2500 μM ATP are indicated. ATP hydrolysis activity was measured at 25°C. The reaction was initiated by addition of 6 nM $\alpha_3\beta_3\gamma$-rot and the activity was monitored for 1 min. 0 nM (triangle), 3 nM (square) and 5 nM (circle) of ε subunit was then added and the activity in the steady state was determined from the slope from 175 to 200 s following ε subunit addition. (**B**) ATP hydrolysis activity of $\alpha_3\beta_3\gamma$-rot was measured with 5 mM ATP at 25°C. The reaction was initiated by addition of 1.5 nM $\alpha_3\beta_3\gamma$-rot and the activity monitored for 1 min. The indicated concentrations of the ε subunits were then added. (**C**) Time course of the inhibition after addition of the ε subunit shown in (B) was used for calculation of $k_{on}$ of the ε subunit to the complex. The curves are fitted to a single exponential equation: $y = a \times e^{-kobs \times t} + b$, where $a$ and $b$ are constants, and $k_{obs}$ is the observed binding rate constant. The association rate constant $k_{on}$ was then obtained from the slope based on the function, $k_{obs} = k_{on} \times [\varepsilon \text{ subunit}] + k_{off}$.

value, owing to large experimental fluctuations, it was deemed unsuitable for calculation of the $K_D$ value. Instead, the $K_D$ value of 3.6 nM obtained from the inhibition of steady-state ATPase activity by the ε subunit was used, allowing determination of the $k_{off}$ value, which was found to be $1.8 \times 10^{-3}\ s^{-1}$.

### *Inhibition of rotation of the γ subunit by the ε subunit*

The rotation of the γ subunit in the $\alpha_3\beta_3\gamma$-rot complex was observed using a 0.2-μm duplex beads as a probe. The

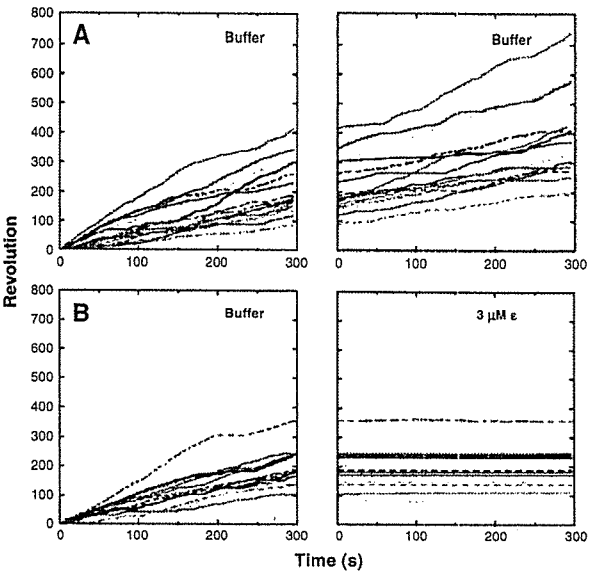


**Figure 5** Effect of the ε subunit on the rotation of the γ subunit in the $\alpha_3\beta_3\gamma$ complex. Rotations of the beads attached to the γ subunit in the presence or the absence of the ε subunit were recorded at 250 nM ATP at 25°C. The buffer without (**A**) or with (**B**) 3 μM ε subunit was infused into the chamber following an initial 5 min observation of rotation. In general, solution exchange in the flow-chamber took 1–2 min. The total number of observed particles was 17 for A (without ε) and 13 for B (with ε).

exchange of the buffer was found to have little effects on the rotation behavior of the γ subunit (Figure 5A). In contrast, significant inhibition of rotation was observed when the ε subunit was injected into the objective chamber (Figure 5B). No continuous rotation was observed on the 13 glass plates examined after injection of the ε subunit, suggesting very tight binding of the ε subunit to the immobilized ATPase molecule and efficient inhibition of the rotation of the γ subunit. From the $k_{off}$ value obtained for the ε subunit, the half-lifetime of the binding of the ε subunit to the complex was calculated as 9.3 min, and the ε subunit could easily rebind to the complex when the concentration of the ε subunit was 3 μM. Therefore, the occasional detachment of the ε subunit from the γ subunit and subsequent resumption of rotation within this experimental period was deemed to be highly unlikely.

### *Analysis of the pause position of the γ subunit caused by the ε inhibition*

When a very low ATP concentration (250 nM) was used for the rotation assay, the movement of the beads attached to the γ subunit showed three discrete pauses, each separated by 120° (Figure 6A). This stepping rotation was not observed when 10 μM ATP was used (Figure 4 in the Supplementary data). The observed 120° pauses can be attributed to ATP binding (Yasuda *et al*, 1998). The angular position of this 120° pause was not significantly affected by the buffer exchange (Figure 6A–C), indicating that the immobilized ATPase complex does not easily undergo a change in position or direction on the glass surface. The average change in pausing angle of the γ subunit from a prior ATP waiting after buffer exchange was 125.3±17.9° (Table I). We next determined the angular position of the pause when rotation was inhibited by the

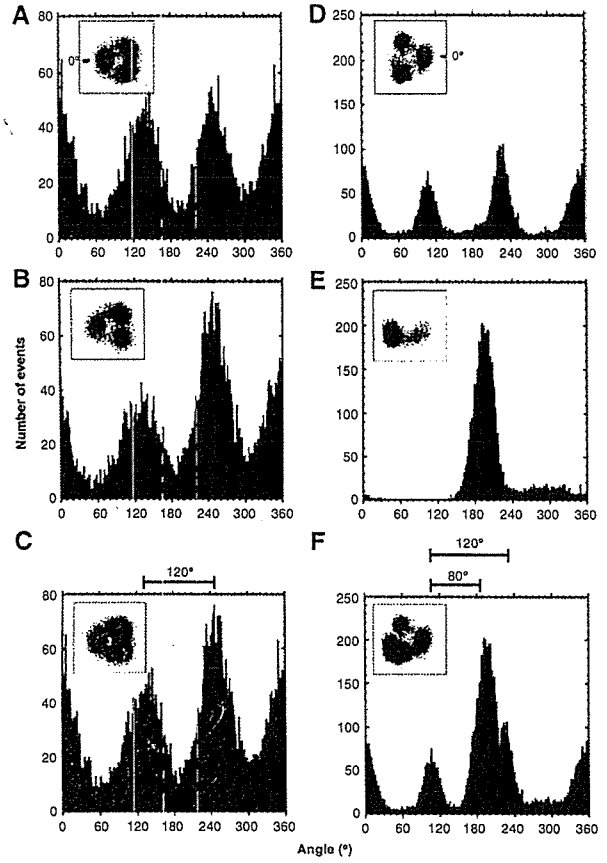


**Figure 6** Stop angular position of the γ subunit inhibited by the ε subunit. Histograms of angular positions of the beads at 250 nM ATP before (**A, D**) and after (**B, E**) buffer exchanges are indicated. (**C, F**) are superimposed histograms of (A, B) and (D, E), respectively. Histograms were taken from rotations observed for 5 min. One of three peak positions of the histogram was set as 0°, and was indicated as the position of the arrow in the traces of the centroid of the beads in the *inset* figures. In the case of the experiments shown in (D–F), buffer containing 3 μM ε subunit was used.

**Table I** Stop angular position of rotation of the γ subunit inhibited by the ε subunit

| Buffer exchange | Pausing angular position of the γ subunit (mean ± s.d.) |
|---|---|
| −ε | 125.3 ± 17.9° ($n$ = 15) |
| +ε | 79.0 ± 20.2° ($n$ = 5) |

The most common location of the bead during rotation is shown as peaks in Figure 6. Each of the peaks was fitted by Gaussian distributions, and the center of the angular position of the γ subunit from the previous ATP binding position (see the peaks in Figure 6B and E) was averaged on the indicated number of the particles.

ε subunit. The location of the beads after the ε injection was clearly limited (Figure 6D–F), and the pausing angle was approximately 80° forward from that for the ATP binding (Table I).

To characterize this 80° pausing position induced by the ε inhibition, we analyzed the slow rotation of the γ subunit of the $\alpha_3\beta_3\gamma$-rot in the presence of 250 nM ATP in detail, and could observe the long pauses (5–45 s) of rotation at 80° from the ATP binding position frequently (Figure 7). These long

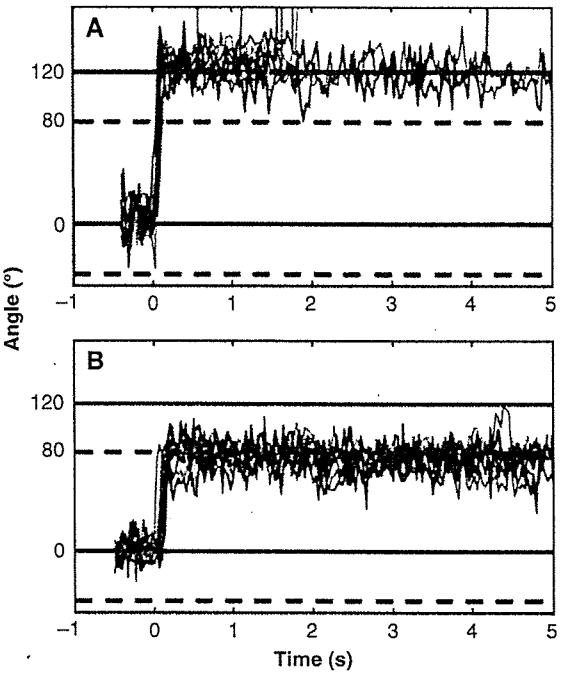


**Figure 7** Long pause of the rotation of the γ subunit at 80°. Pausing angular position of the beads from the ATP waiting position to the next ATP waiting position (**A**) or to the ADP inhibition (**B**) were overlayed ($n$ = 10), when 250 nM ATP was used for the assay.

pauses at 80° seem to be nearly identical to that observed for ADP inhibition state on $TF_1$ (Hirono-Hara *et al*, 2001), suggesting that the pausing angular position by the ε inhibition was identical to that observed for ATP hydrolysis, product release and that for ADP inhibition, but distinctly different from the waiting position for ATP binding.

## Discussion

### *Why can $CF_1$-ε behave as a strong intrinsic inhibitor?*

Based on the observation of the recovery of the ε inhibition of $TF_1$, the ε subunit is thought to exist in two different states in the complex known as the inhibitory state and the non-inhibitory state (Kato-Yamada *et al*, 1999). Based on structural analysis, these two states are considered to be the consequence of the two different ε subunit conformations: the extended conformation and the contracted conformation, respectively (Suzuki *et al*, 2003). Therefore, the transition between these two conformations is thought to be a mode of regulation of the $F_1$-ATPase complex (Suzuki *et al*, 2003; Iino *et al*, 2005). ATP hydrolysis is strongly inhibited in the $F_0F_1$ complex as well, when the ε subunit assumes the extended conformation, in which the C-terminal α-helices of the ε subunit extend into the $\alpha_3\beta_3$ hexagon ring, whereas the contracted ε subunit does not inhibit ATP hydrolysis (Tsunoda *et al*, 2001). The apparent insensitivity of the $TF_1$ or $TF_0TF_1$ to ε inhibition observed in the presence of high concentrations of ATP has therefore been attributed to the contracted conformation of the ε subunit, which is induced by ATP (Kato-Yamada *et al*, 2000, 2005). The ATP-dependent conformational change of the C-terminal α-helical part of ε has also been shown in $EF_0EF_1$ (Schulenberg and Capaldi, 1999).

The results presented here show that, in contrast to the reported ε inhibition of the bacterial $F_1$-ATPase, the inhibitory effect of the ε subunit on the cyanobacterial $\alpha_3\beta_3\gamma$ complex is not influenced by the concentrations of ATP (Figure 1B), suggesting that the drastic conformational changes of the ε subunit from the extended to the contracted conformation is not induced by ATP. This observation is in agreement with the reported inhibitory mechanism of the chloroplast $CF_1$ by the ε subunit (Richter *et al*, 1984). As stated, one of the remarkable differences between the bacterial $F_1$ and $CF_1$ is the existence of an additional ~40 amino acids located in the middle of the γ subunit. Although the γ subunit of the cyanobacterial $F_1$-ATPase is not redox sensitive, it also contains a 26 amino-acid addition whose sequences are very similar to those of $CF_1$-γ. The additional region of the cyanobacterial and chloroplast γ subunit (Hisabori *et al*, 2003) may interfere with the conformational change of the ε subunit, thus $CF_1$-ε can be thought of more as a stationary inhibitory subunit rather than a regulatory one like the bacterial type ε-subunit. In the case of $CF_1$, the thiol modulation system constitutes an additional regulatory mechanism of enzyme activity (Nalin and McCarty, 1984), and this regulation ability seemed to be conferred by the molecular evolution of the additional region of the cyanobacterial γ subunit. In plants, this kind of redox regulation mechanism is likely to be of greater importance because $CF_1$ activity can be linked both to the photochemical reactions and electron transport, thus constituting an effective mechanism for the efficient use of light as an energy source for ATP synthesis.

### *Relation between ε inhibition and ADP inhibition*

The pausing period observed at 80° is considered to encompass the two sequential events; ATP hydrolysis (Shimabukuro *et al*, 2003) and product release (Yasuda *et al*, 2001). Nishizaka *et al* (2004) recently reported that ATP hydrolysis and/or phosphate release but not ADP release would occur at this 80° pause position. In addition, the $TF_1$ subcomplex showed extended pauses at this angular position caused by ADP inhibition (Hirono-Hara *et al*, 2001).

Feniouk and Junge (2005) recently proposed that the ε subunit acts as a stabilizer of the ADP inhibition state in the $F_0F_1$ complex. As the $\alpha_3\beta_3\gamma$ subcomplex also lapses into the ADP inhibition state, ADP inhibition and ε inhibition are independent phenomena. However, our results suggest that these two inhibitions may be tightly linked to each other. In this study, we succeeded in determining the discrete stop position caused by the ε-induced inhibition of rotation, and found it to be approximately 80° forward from the pause position for ATP binding (Figure 6, Table I), confirming that binding of the ε subunit may stabilize ADP inhibition. This conclusion is further supported by the results showing that enzyme activation by LADO was less marked following deletion of additional region of the γ subunit, and this deletion affects ε inhibition (Figure 3).

## Materials and methods

### *Materials*

Biotin-$PEAC_5$-maleimide was purchased from Dojindo (Kumamoto, Japan). ATP, phospho*enol*pyruvate and bovine serum albumin (BSA) were obtained from Sigma. Pyruvate kinase, lactate dehydrogenase and nicotinamide adenine dinucleotide (reduced form) (NADH) were purchased from Roche Diagnostics. Other chemicals were of the highest grade commercially available.

### *Strains and plasmid*

*E. coli* strains used were JM 109 (TAKARA) for cloning and BL21(DE3)*uncΔ702* ($Tc^r$, ATPase mutant, BL21(DE3) *uncΔ702*, asnA::Tn10) (Joshi *et al*, 1989; Nichols and Harwood, 1997) for expression of *T. elongatus* $\alpha_3\beta_3\gamma$. *E. coli* BL21(DE3)*uncΔ*702 strain was kindly gifted from Dr Harwood (University of Iowa). A plasmid pTR19, the expression vector for $F_0F_1$ of thermophilic *Bacillus* PS3 (Suzuki *et al*, 2002), was used as a template to construct the expression vector for *T. elongatus* $\alpha_3\beta_3\gamma$.

### *Construction of expression plasmids for $\alpha_3\beta_3\gamma$ and ε of T. elongatus BP-1*

A 948 base pair DNA fragment containing *atpC* gene, coding for γ subunit of $F_0F_1$, was amplified by polymerase chain reaction (PCR) from genomic DNA of *T. elongatus* BP-1, (a kind gift from Masahiko Ikeuchi, University of Tokyo), using primers 5′-CCGCGGGAATTCGC TTTGCTTAGGAGTTTAAATTACCATGGCCAATCTCAAAGC-3′ (*Eco*RI) and 5′-CGCCGGCGGTACCGCTAGCGCAGAGCCTCAGCCCC-3′ (*Nhe*I). The restriction sites for the enzyme shown in parentheses are underlined. A 1512 base pair DNA fragment containing *atpA* gene, coding for α subunit was amplified using primers 5′-GGCGGC GCCATGGAATCTAAGAAGGAGATATACATATGGTAAGTATCCGACCCG ACG-3′ (*Nco*I) and 5′-CCGCGCCGAATTCTTAGGCAGTGAAGGTAGCT TTGTAC-3′ (*Eco*RI). A 1449 base pair DNA fragment containing *atpB* gene, coding for β subunit of $F_0F_1$, was amplified by PCR using primers 5′-GGCGGGCGCTAGCATTATGAAGGAGATTAATCAAATGCA TCACCATCATCACCATCACCATCACCATATGGTCATATCAGCAGAACG AACC-3′ · (*Nhe*I) and 5′-CCCGCGGAAGCTTCTAAATCTCGACCA CACCCCCTGCG-3′ (*Hin*dIII). These three DNA fragments for α, β and γ subunits were then ligated into the pTR19 plasmids using the restriction enzymes indicated. Consequently, the genes for $TF_0TF_1$ subunits were removed from the plasmid and the plasmid was converted to the expression plasmid for the $\alpha_3\beta_3\gamma$ complex of *T. elongatus*. The obtained plasmid was named pTR19FW.

For the ε subunit expression plasmid, a 417 base pair DNA fragment containing *atpH* gene, coding for the ε subunit of $F_0F_1$, was amplified by PCR from genomic DNA of *T. elongatus* BP-1 using primers 5′-GGCGGGCATATGGTGATGACTGTCCGGGTAATTG CG-3′ (*Nde*I) and 5′-CCCGCGGAAGCTTCTAAATCTCGACCACACCC CCTGCG-3′ (*Hin*dIII). The PCR fragment was digested with *Nde*I and *Hin*dIII and ligated into the plasmid pET21c (Novagen).

### *Mutant complex preparation*

Additional region on the γ subunit corresponding to amino acids 198–222 was deleted from the γ subunit gene on the expression plasmid for $\alpha_3\beta_3\gamma$ using the Mega-primer method (Landt *et al*, 1990) with the following mutation primers: 5′-GCTCCCCCTCGATCCC CAAGGGACCTCGACGCTGCCGCTCTGC-3′. The obtained plasmid was used for the expression of the $\alpha_3\beta_3\gamma_{\Delta198-222}$ complex.

To use the $\alpha_3\beta_3\gamma$ complex for single molecule experiments, all cysteines on the complex were substituted with serine by the Mega-primer method using the following mutation primers: 5′-CCCCTGC ACCTGGTATTGTCCAGCGCAAATCTGTGTCCGAGCCATTGCAAACG GG-3′ for α Cys144Ser; 5′-CCAAAAGGGCCAAGACGTGATTTCCGTG TATGTGGCCATTGGTCAAAAAGCCTCC-3′ for αCys194Ser; 5′-GCGG CCGGCTTAGACGTGGCTGTAACCTCCGAAGTGCAACAACTCC-3′ for βCys53Ser and 5′-GGTGGTAACAGGCGATCGCGGGCTGTCCGGCGG TTACAACACTAATGTCATTCGCCG-3′ for γCys90Ser. Substitutions of Gly112 and Ala125 on γ to Cys for Biotin-$PEAC_5$-Maleimide labeling were carried out by the Mega-primer method using the following mutation primers: 5′-GGAACGTCTCCAAGAACTCGAAGCCGAGTGC CTCAAATACACCCTAGT-3′ for γGly112Cys and 5′-GGGATAGTCACG GCGCTGGAAATATTGGCATGCCTTGCGACCC-3′ for γAla125Cys. In addition, Lys221 on γ was substituted with Ser using the following mutation primers: 5′-CATTTGGAAGTCAACCGCGAGTCGGTAACCTC GACGCTGCCCGCTCTGCCC-3′. The plasmid containing the above mutations was named pTR19FR and used for the expression of $\alpha_3\beta_3\gamma$-rot.

### *Expression and purification of the $\alpha_3\beta_3\gamma$ complex and the ε subunit*

*E. coli* BL21(DE3)*uncΔ702* strain was transformed with pTR19FW or pTR19FR, and cultured in 2 × YT medium containing 100 μg/ml ampicillin and 0.2 mM isopropyl-β-D-thiogalactopyranoside at 37°C

for 19 h. The desired proteins were purified and labeled with Biotin-$PEAC_5$-maleimide by using the same method as described (Ueoka-Nakanishi *et al*, 2004) and stored at −80°C. The ε subunit was expressed and prepared as described (Hisabori *et al*, 1997) and stored at −80°C.

### *Measurement of ATP hydrolysis activity*

ATP hydrolysis activity was measured in the presence of an ATP-regenerating system (Stiggall *et al*, 1979) in 50 mM *N*-2-hydroxyl piperazine-*N'*-2-ethane sulfonic acid (HEPES)-KOH, pH 8.0, 100 mM KCl, 2.5 mM $MgCl_2$, 5 mM ATP, 50 μg/ml pyruvate kinase, 50 μg/ml lactate dehydrogenase, 2 mM phospho*enol*pyruvate and 0.2 mM NADH. The assay was carried out at 25 and 40°C. The rate of ATP hydrolysis after addition of the enzyme was determined by monitoring the decrease in NADH absorption at 340 nm using a spectrophotometer V-550 (Jasco, Tokyo, Japan).

### *Estimation of the ε binding*

The proportion of the complex-bound ε subunit was estimated from the extent of the inhibition of the ATPase activity of the complex. ATP hydrolysis was initiated by addition of the complex to the reaction mixture, monitored for 1 min, and various concentrations of the ε subunit added. The concentration of the $\alpha_3\beta_3\gamma$ complex was fixed at 5 nM. The rate of ATP hydrolysis in steady state was determined from 260 to 280 s after the addition of the ε subunit. The change in the extent of inhibition dependent on the ε concentrations were then fitted with the hyperbolic equation, $y = [(A \times [\varepsilon]_{free})/(K_D + [\varepsilon]_{free})]$, where $y$ represents the percentage of inhibition, $A$ is the maximum inhibition (%) and $K_D$ is the equilibrium dissociation constant for the ε subunit. To calculate the concentration of the free ε subunit, we assumed that the complex that bound an ε subunit is completely inhibited, thus $[\varepsilon]_{free} = [\varepsilon]_{add} - [complex] \times y$.

### *FCS measurement*

$\varepsilon_{Q100C}$ was labeled with Alexa Fluor 488-$C_5$-maleimide (Molecular Probes) with a molar ratio of 1:5 in 100 mM K-phosphate, pH 7.0, 5 mM TCEP and 100 mM KCl at 25°C for 2 h. Unbound fluorescent dye was removed from the solution with NAP5 column (Amersham) equilibrated with 50 mM HEPES-KOH, pH 8.0 and 100 mM KCl. The concentrations of the fluorescent dye bound to the ε subunit was determined from the absorption using excitation coefficient at 493 nm = 72 000 $M^{-1}cm^{-1}$ for the dye. The concentrations of the ε subunit were determined by BCA protein assay. FCS measurements were performed using ConfoCor2 (Carl Zeiss, Jena, Germany) as described (Pack *et al*, 1999, 2000). The sample was excited with 62.5 μW of laser power. To prevent nonspecific adsorption of proteins on the surface of the cover glass, the sample chamber was treated with a protein blocker (N101, NOF Corporation, Japan) before measurement. The measured fluorescence autocorrelation functions were fitted by two-component model as described (Pack *et al*, 2000). In the titration experiment, the duration of measurement was 60 s, and each point on the titration curve is represented by the average of three independent measurements. The titration curves obtained in this study were then fitted with a hyperbolic equation, $y = [(B \times [\varepsilon]_{free})/(K_D + [\varepsilon]_{free})]$, where $y$ represents the % of the binding of the complex to the ε subunit, $B$ is the maximum occupancy of ε with the complex (%) and $K_D$ is the dissociation constant for the ε subunit. As the concentrations of the complex that bound to the ε subunit are obtained directly from the FCS measurement, the concentration of the free ε subunit was calculated as $[\varepsilon]_{free} = [\varepsilon]_{add} - [complex]_{bound}$.

### *Rotation assay*

Biotinylated complexes (10 μl) in 20 mM K-phosphate, pH 7.0, 100 mM KCl and 0.2% (w/v) BSA were infused into a flow chamber and were incubated for 2 min at room temperature. The flow chamber was then washed with 50 μl of 20 mM K-phosphate, pH 7.0 and 100 mM KCl to remove unattached complexes. A streptoavidin beads (209 nm) in 20 mM K-phosphate, pH 7.0, 100 mM KCl and 0.2% (w/v) BSA were infused into the flow chamber and were incubated for 15 min. Rotation was initiated by addition of 30 μl of assay buffer (50 mM HEPES-KOH, pH 8.0, 100 mM KCl, 0.5 mM $MgCl_2$, 250 nM ATP, 100 μg/ml pyruvate kinase and 2 mM phospho*enol*pyruvate) after washing the flow chamber with 50 μl of 50 mM HEPES-KOH, pH 8.0 and 100 mM KCl. The rotation was monitored for 5 min after which the assay buffer containing 3 μM of the ε subunit was infused into the flow chamber to inhibit the enzyme. Rotation of the attached 209 nm duplex beads on the γ subunit was monitored with a conventional optical microscope type IX 71 (Olympus, Tokyo, Japan) with a ×100 objective lens and the images were recorded into a digital video recorder. Recorded images were analyzed by custom software prepared by Yasuda *et al* (1998).

### *Supplementary data*

Supplementary data are available at *The EMBO Journal* Online (http://www.embojournal.org).

## Acknowledgements

We thank Dr C S Harwood (University of Iowa), Dr M Ikeuchi (University of Tokyo), Dr T Suzuki and Dr M Yoshida (ATP System Project, ERATO, JST) for providing us the suitable experimental materials. We also thank Dr B Feniouk, Dr K Yokoyama, Dr H Imamura, Dr R Iino, Dr K Shimabukuro, Dr E Muneyuki, Dr K Motohashi, Dr Y Nakanishi, Dr T Masaike, Dr H Ueno, Ms M Takeda and Dr PGN Romano for fruitful discussions. This work was supported in part by ATP System Project, ERATO, JST, and in part by a Grant-in-aid for Scientific Research (No. 17370015 and No. 17GS0316 to TH) from the Ministry of Education, Culture, Sports, Science and Technology, Japan and by the Japan Society for the Promotion of Science.

## References

Abrahams JP, Leslie AG, Lutter R, Walker JE (1994) Structure at 2.8 Å resolution of $F_1$-ATPase from bovine heart mitochondria. *Nature* **370**: 621–628

Aggeler R, Capaldi RA (1996) Nucleotide-dependent movement of the ε subunit between α and β subunits in the *Escherichia coli* $F_1F_o$-type ATPase. *J Biol Chem* **271**: 13888–13891

Bald D, Amano T, Muneyuki E, Pitard B, Rigaud JL, Kruip J, Hisabori T, Yoshida M, Shibata M (1998) ATP synthesis by $F_oF_1$-ATP synthase independent of noncatalytic nucleotide binding sites and insensitive to azide inhibition. *J Biol Chem* **273**: 865–870

Bar-Zvi D, Shavit N (1982) Modulation of the chloroplast ATPase by tight ADP binding. Effect of uncouplers and ATP. *J Bioenerg Biomembr* **14**: 467–478

Boyer PD (1997) The ATP synthase—a splendid molecular machine. *Annu Rev Biochem* **66**: 717–749

Digel JG, Kishinevsky A, Ong AM, McCarty RE (1996) Differences between two tight ADP binding sites of the chloroplast coupling factor 1 and their effects on ATPase activity. *J Biol Chem* **271**: 19976–19982

Du Z, Tucker WC, Richter ML, Gromet-Elhanan Z (2001) Assembled $F_1$-(αβ) and hybrid $F_1$-$\alpha_3\beta_3\gamma$-ATPases from *Rhodospirillum rubrum* α, wild type or mutant β, and chloroplast γ subunits. Demonstration of $Mg^{2+}$ versus $Ca^{2+}$-induced differences in catalytic site structure and function. *J Biol Chem* **276**: 11517–11523

Duncan TM, Bulygin VV, Zhou Y, Hutcheon ML, Cross RL (1995) Rotation of subunits during catalysis by *Escherichia coli* $F_1$-ATPase. *Proc Natl Acad Sci USA* **92**: 10964–10968

Feldman RI, Boyer PD (1985) The role of tightly bound ADP on chloroplast ATPase. *J Biol Chem* **260**: 13088–13094

Feniouk BA, Junge W (2005) Regulation of the $F_oF_1$-ATP synthase: the conformation of subunit ε might be determined by directionality of subunit γ rotation. *FEBS Lett* **579**: 5114–5118

Grubmeyer C, Cross RL, Penefsky HS (1982) Mechanism of ATP hydrolysis by beef heart mitochondrial ATPase. Rate constants for elementary steps in catalysis at a single site. *J Biol Chem* **257**: 12092–12100

Hirono-Hara Y, Ishizuka K, Kinosita Jr K, Yoshida M, Noji H (2005) Activation of pausing $F_1$ motor by external force. *Proc Natl Acad Sci USA* **102**: 4288–4293

Hirono-Hara Y, Noji H, Nishiura M, Muneyuki E, Hara KY, Yasuda R, Kinosita Jr K, Yoshida M (2001) Pause and rotation of $F_1$-ATPase during catalysis. *Proc Natl Acad Sci USA* **98**: 13649–13654

Hisabori T, Kato Y, Motohashi K, Kroth-Pancic P, Strotmann H, Amano T (1997) The regulatory functions of the γ and ε subunits from chloroplast $CF_1$ are transferred to the core complex, $\alpha_3\beta_3$, from thermophilic bacterial $F_1$. *Eur J Biochem* **247:** 1158–1165

Hisabori T, Kondoh A, Yoshida M (1999) The γ subunit in chloroplast $F_1$-ATPase can rotate in a unidirectional and counter-clockwise manner. *FEBS Lett* **463:** 35–38

Hisabori T, Motohashi K, Kroth P, Strotmann H, Amano T (1998) The formation or the reduction of a disulfide bridge on the γ subunit of chloroplast ATP synthase affects the inhibitory effect of the ε subunit. *J Biol Chem* **273:** 15901–15905

Hisabori T, Ueoka-Nakanishi H, Konno H, Koyama F (2003) Molecular evolution of the modulator of chloroplast ATP synthase: origin of the conformational change dependent regulation. *FEBS Lett* **545:** 71–75

Iino R, Murakami T, Iizuka S, Kato-Yamada Y, Suzuki T, Yoshida M (2005) Real-time monitoring of conformational dynamics of the ε subunit in $F_1$-ATPase. *J Biol Chem* **280:** 40130–40134

Jiang W, Hermolin J, Fillingame RH (2001) The preferred stoichiometry of c subunits in the rotary motor sector of *Escherichia coli* ATP synthase is 10. *Proc Natl Acad Sci USA* **98:** 4966–4971

Joshi AK, Ahmed S, Ferro-Luzzi Ames G (1989) Energy coupling in bacterial periplasmic transport systems. Studies in intact *Escherichia coli* cells. *J Biol Chem* **264:** 2126–2133

Kaibara C, Matsui T, Hisabori T, Yoshida M (1996) Structural asymmetry of $F_1$-ATPase caused by the γ subunit generates a high affinity nucleotide binding site. *J Biol Chem* **271:** 2433–2438

Kato Y, Matsui T, Tanaka N, Muneyuki E, Hisabori T, Yoshida M (1997) Thermophilic $F_1$-ATPase is activated without dissociation of an endogenous inhibitor, ε subunit. *J Biol Chem* **272:** 24906–24912

Kato-Yamada Y (2005) Isolated ε subunit of Bacillus subtilis $F_1$-ATPase binds ATP. *FEBS Lett* **579:** 6875–6878

Kato-Yamada Y, Bald D, Koike M, Motohashi K, Hisabori T, Yoshida M (1999) ε subunit, an endogenous inhibitor of bacterial $F_1$-ATPase, also inhibits $F_oF_1$-ATPase. *J Biol Chem* **274:** 33991–33994

Kato-Yamada Y, Noji H, Yasuda R, Kinosita Jr K, Yoshida M (1998) Direct observation of the rotation of ε subunit in $F_1$-ATPase. *J Biol Chem* **273:** 19375–19377

Kato-Yamada Y, Yoshida M, Hisabori T (2000) Movement of the helical domain of the ε subunit is required for the activation of thermophilic $F_1$-ATPase. *J Biol Chem* **275:** 35746–35750

Krenn BE, Aardewijn P, Van Walraven HS, Werner-Grune S, Strotmann H, Kraayenhof R (1995) ATP synthase from a cyanobacterial *Synechocystis* 6803 mutant containing the regulatory segment of the chloroplast γ subunit shows thiol modulation. *Biochem Soc Trans* **23:** 757–760

Landt O, Grunert HP, Hahn U (1990) A general method for rapid site-directed mutagenesis using the polymerase chain reaction. *Gene* **96:** 125–128

Malyan AN, Vitseva OI (1983) Presteady-state kinetics of ATP hydrolysis by chloroplast $CF_1$-ATPase. *Biokhimiia* **48:** 718–724

Matsui T, Muneyuki E, Honda M, Allison WS, Dou C, Yoshida M (1997) Catalytic activity of the $\alpha_3\beta_3\gamma$ complex of $F_1$-ATPase without noncatalytic nucleotide binding site. *J Biol Chem* **272:** 8215–8221

Meier T, Polzer P, Diederichs K, Welte W, Dimroth P (2005) Structure of the rotor ring of F-type $Na^+$-ATPase from *Ilyobacter tartaricus*. *Science* **308:** 659–662

Minkov IB, Fitin AF, Vasilyeva EA, Vinogradov AD (1979) $Mg^{2+}$-induced ADP-dependent inhibition of the ATPase activity of beef heart mitochondrial coupling factor $F_1$. *Biochem Biophys Res Commun* **89:** 1300–1306

Mitome N, Suzuki T, Hayashi S, Yoshida M (2004) Thermophilic ATP synthase has a decamer c-ring: indication of noninteger 10:3 $H^+$/ATP ratio and permissive elastic coupling. *Proc Natl Acad Sci USA* **101:** 12159–12164

Nakanishi-Matsui M, Kashiwagi S, Hosokawa H, Cipriano DJ, Dunn SD, Wada Y, Futai M (2005) Stochastic high-speed rotation of *Escherichia coli* ATP synthase $F_1$ sector: the ε subunit-sensitive rotation. *J Biol Chem* **280:** 23797–23801

Nalin CM, McCarty RE (1984) Role of a disulfide bond in the γ subunit in activation of the ATPase of chloroplast coupling factor 1. *J Biol Chem* **259:** 7275–7280

Nelson N, Nelson H, Racker E (1972) Partial resolution of the enzymes catalyzing photophosphorylation. XII. Purification and properties of an inhibitor isolated from chloroplast coupling factor 1. *J Biol Chem* **247:** 7657–7662

Nichols NN, Harwood CS (1997) PcaK, a high-affinity permease for the aromatic compounds 4-hydroxybenzoate and protocatechuate from *Pseudomonas putida*. *J Bacteriol* **179:** 5056–5061

Nishizaka T, Oiwa K, Noji H, Kimura S, Muneyuki E, Yoshida M, Kinosita Jr K (2004) Chemomechanical coupling in $F_1$-ATPase revealed by simultaneous observation of nucleotide kinetics and rotation. *Nat Struct Mol Biol* **11:** 142–148

Noji H, Hasler K, Junge W, Kinosita Jr K, Yoshida M, Engelbrecht S (1999) Rotation of *Escherichia coli* $F_1$-ATPase. *Biochem Biophys Res Commun* **260:** 597–599

Noji H, Yasuda R, Yoshida M, Kinosita Jr K (1997) Direct observation of the rotation of $F_1$-ATPase. *Nature* **386:** 299–302

Nowak KF, Tabidze V, McCarty RE (2002) The C-terminal domain of the ε subunit of the chloroplast ATP synthase is not required for ATP synthesis. *Biochemistry* **41:** 15130–15134

Omote H, Sambonmatsu N, Saito K, Sambongi Y, Iwamoto-Kihara A, Yanagida T, Wada Y, Futai M (1999) The γ-subunit rotation and torque generation in $F_1$-ATPase from wild-type or uncoupled mutant *Escherichia coli*. *Proc Natl Acad Sci USA* **96:** 7780–7784

Pack CG, Aoki K, Taguchi H, Yoshida M, Kinjo M, Tamura M (2000) Effect of electrostatic interactions on the binding of charged substrate to GroEL studied by highly sensitive fluorescence correlation spectroscopy. *Biochem Biophys Res Commun* **267:** 300–304

Pack CG, Nishimura G, Tamura M, Aoki K, Taguchi H, Yoshida M, Kinjo M (1999) Analysis of interaction between chaperonin GroEL and its substrate using fluorescence correlation spectroscopy. *Cytometry* **36:** 247–253

Paik SR, Yokoyama K, Yoshida M, Ohta T, Kagawa Y, Allison WS (1993) The $TF_1$-ATPase and ATPase activities of assembled $\alpha_3\beta_3\gamma$, $\alpha_3\beta_3\gamma\delta$, and $\alpha_3\beta_3\gamma\varepsilon$ complexes are stimulated by low and inhibited by high concentrations of rhodamine 6G whereas the dye only inhibits the $\alpha_3\beta_3$, and $\alpha_3\beta_3\delta$ complexes. *J Bioenerg Biomembr* **25:** 679–684

Richter ML, Patrie WJ, McCarty RE (1984) Preparation of the ε subunit and ε subunit-deficient chloroplast coupling factor 1 in reconstitutively active forms. *J Biol Chem* **259:** 7371–7373

Sabbert D, Engelbrecht S, Junge W (1996) Intersubunit rotation in active F-ATPase. *Nature* **381:** 623–625

Schulenberg B, Capaldi RA (1999) The ε subunit of the $F_1F_o$ complex of *Escherichia coli*. Cross-linking studies show the same structure *in situ* as when isolated. *J Biol Chem* **274:** 28351–28355

Seelert H, Poetsch A, Dencher NA, Engel A, Stahlberg H, Muller DJ (2000) Structural biology. Proton-powered turbine of a plant motor. *Nature* **405:** 418–419

Senior AE (1990) The proton-translocating ATPase of *Escherichia coli*. *Annu Rev Biophys Biophys Chem* **19:** 7–41

Shimabukuro K, Yasuda R, Muneyuki E, Hara KY, Kinosita Jr K, Yoshida M (2003) Catalysis and rotation of $F_1$ motor: cleavage of ATP at the catalytic site occurs in 1 ms before 40° substep rotation. *Proc Natl Acad Sci USA* **100:** 14731–14736

Steinemann D, Engelbrecht S, Lill H (1995) Reassembly of *Synechocystis* sp. *PCC* 6803 $F_1$-ATPase from its over-expressed subunits. *FEBS Lett* **362:** 171–174

Stiggall DL, Galante YM, Hatefi Y (1979) Preparation and properties of complex V. *Methods Enzymol* **55:** 308–315, 819–821

Stock D, Leslie AG, Walker JE (1999) Molecular architecture of the rotary motor in ATP synthase. *Science* **286:** 1700–1705

Suzuki T, Murakami T, Iino R, Suzuki J, Ono S, Shirakihara Y, Yoshida M (2003) $F_oF_1$-ATPase/synthase is geared to the synthesis mode by conformational rearrangement of ε subunit in response to proton motive force and ADP/ATP balance. *J Biol Chem* **278:** 46840–46846

Suzuki T, Ueno H, Mitome N, Suzuki J, Yoshida M (2002) $F_o$ of ATP synthase is a rotary proton channel. Obligatory coupling of proton translocation with rotation of c-subunit ring. *J Biol Chem* **277:** 13281–13285

Tsunoda SP, Rodgers AJ, Aggeler R, Wilce MC, Yoshida M, Capaldi RA (2001) Large conformational changes of the ε subunit in the bacterial $F_1F_o$ ATP synthase provide a ratchet action to regulate this rotary motor enzyme. *Proc Natl Acad Sci USA* **98:** 6560–6564

Ueoka-Nakanishi H, Nakanishi Y, Konno H, Motohashi K, Bald D, Hisabori T (2004) Inverse regulation of rotation of $F_1$-ATPase by the mutation at the regulatory region on the γ subunit of chloroplast ATP synthase. *J Biol Chem* **279:** 16272–16277

Vasilyeva EA, Minkov IB, Fitin AF, Vinogradov AD (1982) Kinetic mechanism of mitochondrial adenosine triphosphatase. ADP-specific inhibition as revealed by the steady-state kinetics. *Biochem J* **202:** 9–14

Werner-Grune S, Gunkel D, Schumann J, Strotmann H (1994) Insertion of a 'chloroplast-like' regulatory segment responsible for thiol modulation into γ-subunit of $F_oF_1$-ATPase of the cyanobacterium *Synechocystis* 6803 by mutagenesis of atpC. *Mol Gen Genet* **244:** 144–150

Yasuda R, Noji H, Kinosita Jr K, Yoshida M (1998) $F_1$-ATPase is a highly efficient molecular motor that rotates with discrete 120° steps. *Cell* **93:** 1117–1124

Yasuda R, Noji H, Yoshida M, Kinosita Jr K, Itoh H (2001) Resolution of distinct rotational substeps by submillisecond kinetic analysis of $F_1$-ATPase. *Nature* **410:** 898–904

Yoshida M, Muneyuki E, Hisabori T (2001) ATP synthase—a marvellous rotary engine of the cell. *Nat Rev Mol Cell Biol* **2:** 669–677

Yoshida M, Sone N, Hirata H, Kagawa Y, Ui N (1979) Subunit structure of adenosine triphosphatase. Comparison of the structure in thermophilic bacterium PS3 with those in mitochondria, chloroplasts, and *Escherichia coli*. *J Biol Chem* **254:** 9525–9533

Zhou JM, Xue ZX, Du ZY, Melese T, Boyer PD (1988) Relationship of tightly bound ADP and ATP to control and catalysis by chloroplast ATP synthase. *Biochemistry* **27:** 5129–5135

Zimmermann B, Diez M, Zarrabi N, Graber P, Borsch M (2005) Movements of the ε-subunit during catalysis and activation in single membrane-bound $H^+$-ATP synthase. *EMBO J* **24:** 2053–2063

J|A|C|S
COMMUNICATIONS

Published on Web 07/04/2006

# Control of the Optical Properties of Quantum Dots by Surface Coating with Calix[*n*]arene Carboxylic Acids

Takashi Jin,*,† Fumihiko Fujii,† Eiji Yamada,‡ Yoshinobu Nodasaka,§ and Masataka Kinjo†

*Research Institute for Electronic Science, Hokkaido University, Sapporo 060-0812, Japan, Faculty of Engineering, Hokkaido University, Sapporo 060-8628, Japan, and Faculty of Dental Medicine, Hokkaido University, Sapporo 060-8586, Japan*

Received March 24, 2006; E-mail: jin@imd.es.hokudai.ac.jp

Semiconductor quantum dots (QDs) have become a new class of fluorescent probes that can be used for biological labeling,[1] in vivo bioimaging,[2] and multi-color optical encoding of biomolecules.[3] Since the optical properties of semiconductor QDs can be continuously tuned by changing the particle size, a variety of QDs (II−IV and III−V semiconductor materials) that emit in the visible to the near-infrared regions have been developed.[4] Recent advances in the synthesis of QDs have led to the development of smaller QDs,[5,6] where the optical properties can be tunable without a change in the particle size.[6] Several groups have reported alloyed semiconductor QDs for size-independent tuning of the emission properties.[6] Bailey and Nie showed that the emission peaks of ternary $CdSe_xTe_{1-x}$ QDs can be controlled by varying the composition of Se and Te.[6c] Here, we report a new method for the control of the optical properties of CdSe/ZnS (core−shell) QDs by changing the surface coating layer with different oligomer sizes of calixarene derivatives.

Recently, we have found that the surface of CdSe/ZnS QDs can be modified with amphiphilic calixarene derivatives to give water-soluble QDs.[7] In this work, we examined the optical properties of CdSe/ZnS QDs coated with calix[*n*]arene carboxylic acids (**1**−**3**). The calixarene coating was performed by mixing trioctylphosphine oxide (TOPO)-capped CdSe/ZnS QDs and **1**−**3** in tetrahydrofuran at room temperature. Deprotonation of the carboxyl groups of the calix[*n*]arene resulted in water-soluble QDs (Scheme 1). The QDs were highly fluorescent (quantum yield = 0.1−0.34) and stable for more than 1 month in aqueous solution.

***Scheme 1.*** Preparation of Water-Soluble CdSe/ZnS QDs by Surface Coating with Calix[*n*]arene Carboxylic Acids (**1**−**3**)

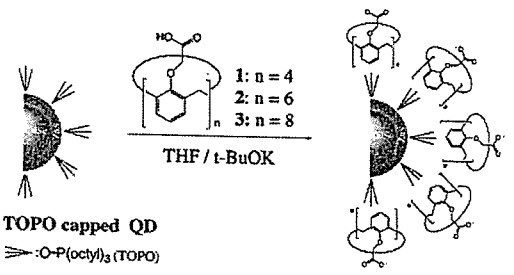


Figure 1a−c shows the fluorescence spectra of CdSe/ZnS QDs before and after the surface coating with **1**−**3**. The emission peak of QDs shifted to longer wavelengths with increasing the oligomer size of the calix[*n*]arene used. In the case of the CdSe/ZnS QD with a 530 nm emission peak, the red shifts were observed to be 8, 21, and 35 nm for **1**-, **2**-, and **3**-coated QDs, respectively. When the QDs with longer emission peaks were coated, the red shifts became smaller. The dependences of oligomer sizes of the calixarene on the peak shifts are shown in Figure 1d. The result indicates that the emission peaks of CdSe/ZnS QDs can be controlled by the surface coating of the QDs with calix[*n*]arene carboxylic derivatives.

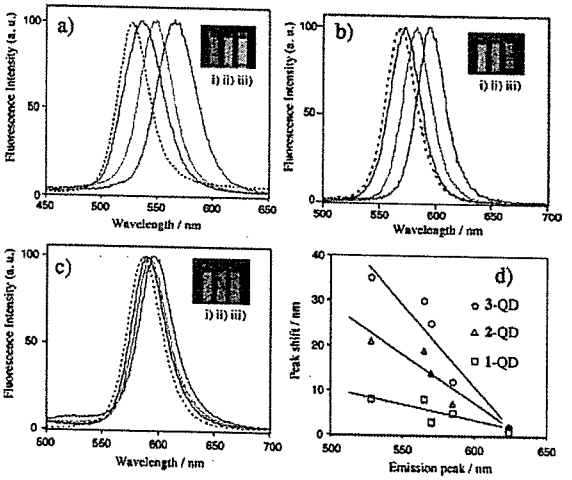


***Figure 1.*** Fluorescence spectra (a−c) of TOPO-capped CdSe/ZnS QDs in chloroform (broken line) and their surface-coated QDs with **1**−**3** in water (blue for **1**, green for **2**, and red for **3**). The inset shows the fluorescence image of the calix[*n*]arene-coated QDs exited at 365 nm (i for **1**-QD, ii for **2**-QD, and iii for **3**-QD). The peak shifts of the calix[*n*]arene-coated QDs compared to the initial QDs are shown in (d).

To understand the mechanism of the red shifts, we first examined the absorption spectra of the QDs. Figure 2a shows the absorption spectra of TOPO-capped QDs (565 nm emission) and their surface-coated QDs with **1**−**3**. It should be noted that the band edge absorption shifts to longer wavelengths depending on the oligomer size of calixarenes used for the surface coating. This result shows that the band gap energy decreases in the calixarene-coated QDs compared to that of the initial TOPO-capped QDs. It is well-known that the band gap energy in CdSe/ZnS QDs decreases with increasing particle size.[4a] In the calixarene-coated QDs, however, the particle sizes of the CdSe/ZnS moiety could not be changed because the surface coating procedure was performed at room temperature.

To characterize the structure of the calixarene-coated QDs, we determined their particle size using TEM and fluorescence correlation spectroscopy (FCS).[7,8] The inset in Figure 2b shows a TEM image of the TOPO-capped CdSe/ZnS QDs (565 nm emission). The TEM image shows that the size of the core−shell moiety of the QDs is ca. 5 nm. For each of the QDs coated with **1**−**3**, we attempted to measure their particle sizes using TEM, but we failed

† Research Institute for Electronic Science.
‡ Faculty of Engineering.
§ Faculty of Dental Medicine.



10.1021/ja062021k CCC: $33.50 

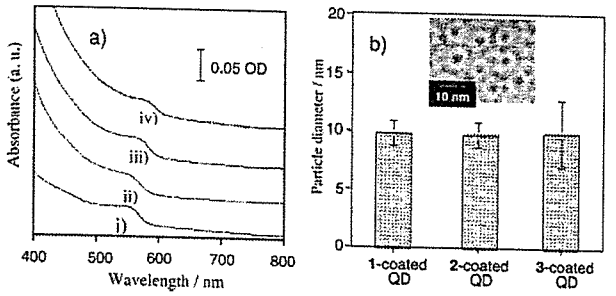


***Figure 2.*** (a) Absorption spectra of CdSe/ZnS QDs (565 nm emission) before and after coating with calix[*n*]arene carboxylic acids: (i) TOPO-coated QDs in chloroform; (ii) **1**-coated QDs; (iii) **2**-coated QDs; and (iv) **3**-coated QDs in water. (b) TEM images (inset) for TOPO-coated QDs (565 nm emission) and the hydrodynamic particle diameter of **1**-, **2**-, and **3**-coated QDs determined by FCS.

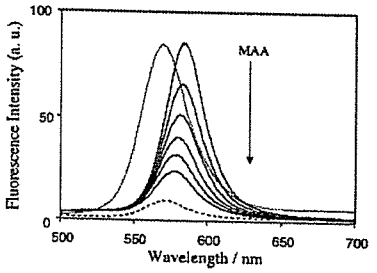


***Figure 3.*** Changes in the fluorescence spectra (solid lines) of **3**-coated CdSe/ZnS QDs by ligand-exchange with mercaptoacetic acid (MAA) in borate buffer (pH = 9.2). MAA was added to the QD solution (o.d. = 0.05 at 480 nm) as an aqueous solution (2 mg/mL). For comparison, the fluorescence spectra of TOPO-capped QDs before coating by **3** in chloroform (red line) and MAA-coated QDs in water (broken line) prepared separately are shown.

to obtain, due to the aggregation during dryness of QD colloids on the Cu grid. Instead, we measured hydrodynamic diameters of the calixarene-coated QDs by using FCS. Interestingly, the hydrodynamic diameters of the QDs were calculated to be similar values (ca. 10 nm) for **1**-, **2**-, and **3**-coated QDs (Figure 2b). This result indicates that the thickness of the organic surface layer is 2.5 nm long for all of the QDs coated with **1**−**3**. The molecular lengths of TOPO and calix[*n*]arene carboxylic acids along their alkyl chains are estimated to be 1.3 and 0.95 nm, respectively. Thus it is reasonable to assume that the surface layer of the QDs forms a bilayer structure, as shown in Scheme 1 (see Supporting Information).

If the surface organic layer induces the emission shifts in the calixarene-coated QDs, their emission properties should be affected by compositions of the surface layer of QDs. To confirm the surface coating effect of **1**−**3** on the optical properties of QDs, we performed a ligand-exchange experiment. The surface organic layer of **3**-coated QDs was exchanged with mercaptoacetic acids (MAA). Figure 3 shows the changes in the fluorescence spectra of **3**-coated QDs upon addition of MAA. With increasing the concentration of MAA, the emission peak of **3**-coated QDs shifted to shorter wavelengths and the emission spectra became close to that of MAA coated QDs. Thus, the red shift observed in the **3**-coated QDs can be attributed to the surface coating effect by the calixarene derivative of **3**.

The theoretical study of the factors that influence the excitonic states in semiconductor QDs has shown that dielectric confinement effects[9] are also important as well as quantum (size) confinement effects.[10] It has been predicted that the change in the dielectric constant of the medium surrounding the QDs results in the change in the exciton binding energy.[9] We believe that the difference in dielectric nature of the surface layer (TOPO and calixarene) plays an important role in the red shifts of the emission of QDs coated with **1**−**3**. Recently, Feng et al. reported a red shift of over 15 nm in the TOPO-capped QDs upon complexation of γ-cyclodextrin, and on the basis of first-principles calculations, they suggested that the S atom in the ZnS shell is exchanged with the hydroxyl oxygen atom of the cyclodextrin.[11] In the case of the calixarene-coated QDs, the possibility that the change of the ZnS surface due to the binding of calixarene derivatives may have resulted in the red shifts cannot be ruled out.

In conclusion, we have presented a new method for the control of the optical properties of QDs by surface coating with the calix[*n*]arene derivatives. Although the coating effect on the shifts of the emission peak of QDs decreases with increasing the particle sizes (emission wavelengths) of QDs, this method is useful for the preparation of water-soluble multi-colored QDs from an initial TOPO-coated QD. We expect that the surface coating method using calix[*n*]arene carboxylic acids can be applied to other semiconductor QDs for the control of the optical properties of QDs without changing the particle sizes.

**Acknowledgment.** We thank Prof. M. Tamura for continual encouragement.

**Supporting Information Available:** Synthetic procedures for **1**−**3** and QDs, surface coating procedure, TEM and FCS measurements, and additional characterization results. This material is available free of charge via the Internet at http://pubs.acs.org.

## References

(1) (a) Bruchez, M., Jr.; Moronne, M.; Gin, P.; Weiss, S.; Alivisantos, A. P. *Science* **1998**, *281*, 2013−2016. (b) Chan, W. C. W.; Nie, S. *Science* **1998**, *281*, 2016−2018.
(2) (a) Gao, X.; Yang, L.; Petros, J. A.; Marshall, F. F.; Simons, J. W.; Nie, S. *Curr. Opin. Biotechnol.* **2005**, *16*, 63−72. (b) Pinaud, F. F.; Michalet, X.; Bentolila, L. A.; Tsay, J. M.; Doose, S.; Li, J. J.; Iyer, G.; Weiss, S. *Biomaterials* **2006**, *27*, 1679−1687.
(3) Han, M.; Gao, X.; Su, J. Z.; Nie, S. *Nat. Biotechnol.* **2001**, *19*, 631−635.
(4) (a) Dabbousi, B. O.; Rodriguez-Viejo, J.; Mikulec, F. V.; Heine, J. R.; Mattoussi, H.; Ober, R.; Jensen, K. F.; Bawendi, M. G. *J. Phys. Chem. B* **1997**, *101*, 9463−9475. (b) Michalet, X.; Pinaud, F. F.; Bentolila, L. A.; Tsay, J. M.; Doose, S.; Li, J. J.; Sundaresan, G.; Wu, A. M.; Gambhir, S. S.; Weiss, S. *Science* **2005**, *28*, 538−544.
(5) Zimmer, J. P.; Kim, S.-W.; Ohnishi, S.; Tanaka, E.; Frangioni, J. V.; Bawendi, M. G. *J. Am. Chem. Soc.* **2006**, *128*, 2526−2527.
(6) (a) Petrov, D. V.; Santos, B. S.; Pereira, G. A.; Donegá, C. D. M. *J. Phys. Chem. B* **2002**, *106*, 5325−5334. (b) Wang, W.; Germanenko, I.; El-Shall, M. S. *Chem. Mater.* **2002**, *14*, 3028−3033. (c) Bailey, R. E.; Nie, S. *J. Am. Chem. Soc.* **2003**, *125*, 7100−7106. (d) Zhong, X.; Feng, Y.; Knoll, W.; Han, M. *J. Am. Chem. Soc.* **2003**, *125*, 13559−13563.
(7) (a) Jin, T.; Fujii, F.; Sakata, H.; Tamura, M.; Kinjo, M. *Chem. Commun.* **2005**, 2829−2831. (b) Jin, T.; Fujii, F.; Sakata, H.; Tamura, M.; Kinjo, M. *Chem. Commun.* **2005**, 4300−4302.
(8) (a) Yoshida, N.; Kinjo, M.; Tamura, M. *Biochem. Biophys. Res. Commun.* **2001**, *280*, 312−318. (b) Tsay, J. M.; Doose, S.; Weiss, S. *J. Am. Chem. Soc.* **2006**, *128*, 1639−1647.
(9) Takagahara, T. *Phys. Rev. B* **1993**, *47*, 4569−4584.
(10) (a) Rosseti, R.; Nakahara, S.; Brus, L. E. *J. Chem. Phys.* **1983**, *79*, 1086−1088. (b) Alivisatos, A. P. *Science* **1996**, *271*, 933−937.
(11) Feng, J.; Ding, S.-K.; Tucker, M. P.; Himmel, M. E.; Kim, Y.-H.; Zhang, S. B.; Keyes, B. M.; Rumbles, G. *Appl. Phys. Lett.* **2005**, *86*, 033108−033111.

JA062021K

FEBS Letters 581 (2007) 389–393

# Analysis of intranuclear binding process of glucocorticoid receptor using fluorescence correlation spectroscopy

Shintaro Mikuni, Mamoru Tamura, Masataka Kinjo*

*Laboratory of Supramolecular Biophysics, Research Institute for Electronic Science, Hokkaido University, N12W6, Kita-ku, Sapporo 060-0812, Japan*

Received 22 September 2006; revised 8 December 2006; accepted 21 December 2006

Available online 18 January 2007

Edited by Frances Shannon

**Abstract The diffusion properties of EGFP-hGRα and mutants C421G, A458T and I566 in living cells were analyzed. The wild type and mutants C421G and A458T translocated from the cytoplasm to the nucleus after addition of Dex; however, the Brownian motions of the proteins were different. The diffusion constant of wild-type GRα after addition of Dex slowed to 15.6% of that in the absence of Dex, whereas those of A458T and C421G slowed to 34.8% and 61.7%, respectively. This is the first report that dimer formation is less important than the binding activity of GRα to GRE in the living cell.**



*Keywords:* Glucocorticoid response element; Diffusion constant; Glucocorticoid receptor; Mutant; Dexamethasone; RU486

## 1. Introduction

Understanding the interactions and dynamic properties of biomolecules and biomolecular networks in living cells is of central importance in life science. Direct observation of the actions of transcription factors in the living cell can provide important insights into gene regulatory mechanisms. We analyzed the diffusion of green fluorescence protein fused human glucocorticoid receptor α (EGFP-hGRα) before and after addition of ligands in the nuclei of living cells using fluorescence correlation spectroscopy (FCS).

The glucocorticoid receptor (GR) is a transcriptional regulatory protein that controls broad physiological gene networks, and has pathological effects in a range of diseases; therefore the protein offers an excellent target for therapeutic intervention [1,2]. GR is associated with several proteins in the absence of ligands in the cytoplasm. The humans GR receptor can be found in two isoforms GRα, and GRβ. GRα consists of 777 amino acids, binds hormones and activates glucorticoid-responsive genes. Upon ligand binding, GRα is driven into the nucleus, and regulates transactivation by association with specific genomic glucocorticoid response elements (GRE).

Various functional domains and many cofactors of GRα have been identified by biochemical and molecular biological methods [3], and dynamics of GRα in the living cell has been analyzed using fluorescence recovery after photobleaching (FRAP) [4–6].

Large studies of FRAP using GFP-tagged proteins have been employed to understand diffusion kinetics of nuclear factors. However, even the sensitivity of conventional fluorescence techniques, including FRAP expanded to the single molecule level, can detect only slow dynamics [7].

FCS has been used to analyze the microenvironment of the cell membrane [8], endoplasmic reticulum [9] and nucleus and nucleolus [10], though the changes in the diffusion (Brownian) motion of fluorophores could not be detected by FRAP because of rapid movement. We have detected a slow-moving component of EGFP-hGRα in the nucleus with the addition of dexamethasone (Dex). To elucidate this slow component, we constructed three hGRα mutants: EGFP-hGRα/C421G (C421G) which cannot associate with GRE [11], EGFP-hGRα/A458T (A458T), with no dimerization ability [12], and EGFP-hGRα/I566 (I566), in which the ligand binding domain (LBD) was deleted to reduce association with some cofactors [1].

## 2. Materials and methods

### 2.1. Chemicals and plasmids

Dexamethasone (Dex) and RU486 were purchased from Sigma (St. Louis, MO, USA). These chemicals were used as ethanol solutions.

Plasmids encoding the hGRα fused with green fluorescent protein (pCMX-hGRα-GFP) were kindly provided by Dr. H. Tanaka [13] and Dr. Y. Nomura [14]. To obtain brighter fluorescence, pEGFP-hGRα was constructed by PCR amplification of hGRα fragments and ligation into pEGFP-C1 (Clontech, Palo Alto, CA, USA). EGFP-hGRα/I566 (I566) and EGFP-hGRα/A458T (A458T) plasmids were constructed by PCR amplification, EGFP-hGRα/C421G (C421G) plasmid was constructed by a two step PCR procedure [15], with primers containing mutations using pEGFP-hGRα as a template. After purification of PCR products, the digested fragments inserted into pEGFP-hGRα were cut with restriction enzymes. The pairs of primers and restriction enzymes for I566, A458T and C421G are shown below:

I566; forward: 5′-AATGATTGCATCATCGATAAAATTCGAAGA-3′,
reverse: 5′-CACTTGGATCCCTCATAACATGTTGAGCGTA-GTC-3′,
restriction enzymes: *Cla*I and *Bam*HI.

A458T; forward: 5′-GGGTCCCCAGGTAAAGAGACGAA-3′,
reverse: 5′-TTTATCGATGATGCAATCATTCCTTCCA-G*T*AC-ATAGGT-3′,
restriction enzymes: *Esp*3I and *Cla*I.

*Corresponding author. Fax: +81 11 706 9006.
*E-mail address:* kinjo@imd.es.hokudai.ac.jp (M. Kinjo).

*Abbreviations:* FCS, fluorescence correlation spectroscopy; FAF, fluorescence autocorrelation function; EGFP, enhanced green fluorescent protein; Dex, dexamethasone; LBD, ligand binding domain; DBD, DNA binding domain; GR, glucocorticoid receptor; GRE, glucocorticoid response element

0014-5793/$32.00 
doi:10.1016/j.febslet.2006.12.038

C421G; forward-1: 5′-GGGTCCCCAGGTAAAGAGACGAA-3′, reverse-1: 5′-CAGAGCACACCAGGCCGAGTTTGGGAGG-3′, and forward-2: 5′-ACCTCCCAAACTCGGCCTGGTGTGCTCTG-3′, reverse-2: 5′-CAGAGGTTTCTTGTGAGACTCCTGTAGTG-3′ restriction enzymes: *Esp*3I and *Cla*I.

All of the above PCRs were performed using KOD-Plus- (TOYOBO, Tokyo, Japan) according to the manufacturer's instructions.

### 2.2. Transient transfection

HeLa cells were transfected using the lipofection reagent FuGENE 6 (Roche Molecular Biochemicals, Mannheim, Germany) with 0.1 μg/well pEGFP-C1, pEGFP-hGRα, pEGFP-hGRα/I566, pEGFP-hGRα/A458T or pEGFP-hGRα/C421G according to the manufacturer's instructions.

### 2.3. FCS measurement and analysis

FCS measurement was performed with a LSM510-ConfoCor2 combination system (Carl Zeiss, Jena, Germany) before and every 10 min after addition of 100 nM of the indicated ligands. Each set of FCS measurements was carried out five times with a duration of 15 s. Fluorescence autocorrelation functions (FAFs, G(τ)) were acquired and fitted with the FCS Fit program by one-, two-, or three-component models as follows:

$$G(\tau) = \frac{\langle I(t)\rangle\langle I(t+\tau)\rangle}{\langle I(t)\rangle^2} = \frac{1 - F_{\text{triplet}} + F_{\text{triplet}}\exp(-\tau/\tau_{\text{triplet}})}{N(1-F_{\text{triplet}})} \times \sum_i \frac{F_i}{(1+\tau/\tau_i)\sqrt{1+\tau/s^2\tau_i}} + 1 \quad (1)$$

where $F_{\text{triplet}}$ is the average fraction of triplet state molecules, $\tau_{\text{triplet}}$ is the triplet relaxation time, $F_i$ and $\tau_i$ are the fraction and diffusion time of component $i$, respectively, $N$ is the number of fluorescence molecules in the detection volume element defined by radius $w_0$ and length $2z_0$, and $s$ is the structural parameter representing the ratio, $s = z_0/w_0$. In this paper, the fluorescence autocorrelation function was shown as normalized by $N$ for comparisons of $\tau$.

$$\text{Normalized } G(\tau) = N(G(\tau) - 1) \quad (2)$$

Diffusion constants of samples were obtained from the ratio with the diffusion constant of R6G and diffusion time $\tau_{\text{R6G}}$ and $\tau_{\text{sample}}$ [8].

## 3. Results and discussion

### 3.1. Mobility of EGFP in the living cell

As shown in Fig. 1A, EGFP was distributed without distinction in the cytoplasm and nucleus even if Dex was added. Similar FAFs were obtained for the nucleus and cytoplasm (Fig. 1B). Most FAFs in the nucleus and cytoplasm could be fitted with a one-component model and the averages of the diffusion constants were calculated to be 20.4 ± 3.2 μm²/s and 19.3 ± 0.9 μm²/s, respectively. This indicated that EGFP did not interact with any proteins or diffuse as free-moving molecules whether in the nucleus or cytoplasm. Moreover, this mobility of EGFP was not affected by addition of ligands (Fig. 1B, C). FAFs in PBS buffer solution could be fitted with the one-component model and the average diffusion constant was calculated to be 72.8 ± 2.8 μm²/s (Fig. 1B), the same as in previous reports [8].

### 3.2. The effect of Dex on the localization and diffusion of EGFP-hGRα

To observe the localization of EGFP-hGRα in HeLa cells, confocal LSM images were taken before and after addition of Dex. EGFP-hGRα was mainly localized in the cytoplasm in the absence of Dex. However, the subcellular localization of EGFP-hGRα was changed to the nucleus by exposure to Dex, a transactivation agonist, within 30 min (Fig. 2A). We also measured FAFs of EGFP-hGRα in the nuclei of the living cells. As shown in Fig. 2B, normalized FAFs were clearly shifted to the right by the presence of Dex in the nucleus. This shift indicated that a slow-moving EGFP-hGRα appeared. Under this concentration of Dex, the slow-moving fraction reached a plateau in 20 min (data not shown). On the other hand, FAFs obtained from the cytoplasm did not differ in the presence and absence of Dex (Fig. 2C).

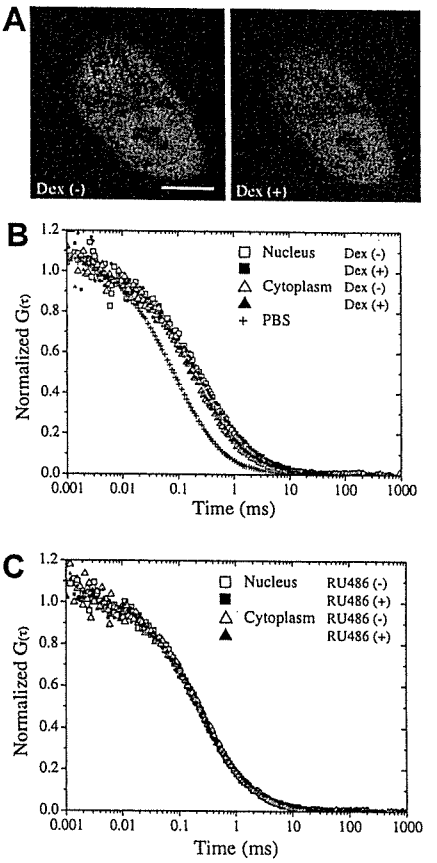


Fig. 1. LSM images and normalized FAFs in a HeLa cell expressing EGFP. (A) A HeLa cell expressing EGFP was imaged before (left) and 60 min after (right) addition of Dex to 100 nM. The scale bar represents 10 μm. (B) FAFs were acquired in PBS buffer (cross) or at the nucleus (square) and cytoplasm (triangle) in HeLa cells expressing EGFP. FCS measurement performed before (open symbols) and 60 min after (closed symbols) addition of 100 nM Dex (C) or RU486.

Most FAFs in the nuclei could be fitted with a two-component model. The average diffusion constants and fractions are summarized in Table 1, which shows that the fractions of each component were not much changed (Table 1, F1 and F2). On the other hand, addition of Dex reduced the diffusion constants of the second component to 15.6% of that in the absence of Dex (Fig. 7). This result could indicate that this slow-moving component originated from the formation of a complex with transcription cofactors and/or interaction with DNA of the activated hGRα. It is noted that the fast component of wild-type GRα decreased in the presence of Dex, this may indicate that an initial complex of GRα and a cofactor could be detected.